SSC-191

PLASTIC FLOW IN THE LOCALE ON NOTCHES AND CRACKS IN Fe-3Si STEEL UNDER CONDITIONS APPPOACHING PLANE STRAIN

SHIP STRUCTURE COMMITTEE

November 1968

SHIP STRUCTURE COMMITTEE

ADDRESS CORRESPONDENCE TO:

SECRETARY
SHIP STRUCTURE COMMITTEE
U.S. COAST GUARD HEADQUARTERS
WASHINGTON, D.C. 20591

November 1968

Dear Sir:

The Ship Structure Committee has completed a three-year study at Battelle Memorial Institute in examining the extent of localized yielding and stress relaxation around a notch, learning how to measure it, and trying to translate the information for use in problems of fracture and design. Herewith is the final report entitled *Plastic Flow In The Locale On Notches And Cracks In Fe-3Si Steel Under Conditions Approaching Plane Strain* by G. T. Hahn and A. R. Rosenfield.

This report is being distributed to individuals and groups associated with or interested in the work of the Ship Structure Committee. Comments concerning this report are solicited.

Sincerely,

D. B. Henderson

D. B. Henderson
Rear Admiral, U. S. Coast Guard
Chairman, Ship Structure Committee

SSC-191

Final Report

on

Project SR-164

"Local Strain Measurement"

to the

Ship Structure Committee

PLASTIC FLOW IN THE LOCALE ON NOTCHES AND CRACKS IN Fe-3Si STEEL UNDER CONDITIONS APPROACHING PLANE STRAIN

by

G. T. Hahn and A. R. Rosenfield

Battelle Memorial Institute
Columbus, Ohio

under

Department of the Navy
Naval Ship Engineering Center
Contract NObs-92383

U. S. Coast Guard Headquarters
Washington, D. C.

ABSTRACT

The development of the plastic zones generated by sharp through-cracks and blunter notches was studied systematically in plates of Fe-3Si steel. A sensitive etching technique revealed the plastic zone both on the plate surface and on parallel and normal interior sections. In addition, the progress of through-the-thickness deformation was followed by monitoring normal displacements at the plate surface. The work encompasses applied stress-crack length-thickness combinations in the range $0.2 < \left|\frac{K}{Y}\right|^2 \frac{1}{t} < 2$ (K is the stress intensity parameter, Y is the Yield stress, and t is the plate thickness), with special emphasis on situations where the plastic zone is small relative to the plate thickness and a plane strain state is approached. Three kinds of relaxations are revealed: one in the plane of the plate and two accomodating through-the-thickness deformation. The latter become the dominant mode when $\left|\frac{K}{Y}\right|^2 \frac{1}{t} > 1.7$ or $\rho \gtrsim \frac{t}{2}$ (ρ is the zone length). Comparisons with available theoretical treatments show that the calculations of Bilby and Swinden, Tuba, and Rice and Rosengren are in accord with measured zone lengths, but none of the treatments examined provides a satisfactory description of the zone shape. The experiments also provide insights to the level of strain within the zone, and suggest that $\left|\frac{K}{Y}\right|^2 \frac{1}{2} = 1$ or $\rho = \frac{t}{4}$ may be a useful upper bound for the plane strain regime.

SHIP STRUCTURE COMMITTEE

The SHIP STRUCTURE COMMITTEE is constituted to prosecute a research program to improve the hull structures of ships by an extension of knowledge pertaining to design, materials and methods of fabrication.

RADM D. B. Henderson, USCG - Chairman
Chief, Office of Engineering
U. S. Coast Guard Headquarters

Captain William R. Riblett
Head, Ship Engineering Division
Naval Ship Engineering Center

Mr. E. Scott Dillon
Chief, Division of Ship Design
Office of Ship Construction
Maritime Administration

Captain T. J. Banvard, USN
Maintenance and Repair Officer
Military Sea Transportation Service

Mr. D. B. Bannerman, Jr.
Vice President - Technical
American Bureau of Shipping

SHIP STRUCTURE SUBCOMMITTEE

The SHIP STRUCTURE SUBCOMMITTEE acts for the Ship Structure Committee on technical matters by providing technical coordination for the determination of goals and objectives of the program, and by evaluating and interpreting the results in terms of ship structural design, construction and operation.

NAVAL SHIP ENGINEERING CENTER

Mr. J. J. Nachtsheim - Chairman
Mr. John Vasta - Contract Administrator
Mr. George Sorkin - Member
Mr. Harrison S. Sayre - Alternate
Mr. Ivo Fioriti - Alternate

MARITIME ADMINISTRATION

Mr. Frank Dashnaw - Member
Mr. Anatole Maillar - Member
Mr. R. Falls - Alternate
Mr. W. G. Frederick - Alternate

AMERICAN BUREAU OF SHIPPING

Mr. G. F. Casey - Member
Mr. F. J. Crum - Member

OFFICE OF NAVAL RESEARCH

Mr. J. M. Crowley - Member
Dr. Wm. G. Rauch - Alternate

MILITARY SEA TRANSPORTATION SERVICE

LCDR R. T. Clark, USN - Member
Mr. R. R. Askren - Member

U. S. COAST GUARD

CDR C. R. Thompson, USCG - Member
CDR J. L. Howard, USCG - member
LCDR Leroy C. Melberg, USCG - Alternate
LCDR R. L. Brown, USCG - Alternate

NAVAL SHIP RESEARCH & DEVELOPMENT CENTER

Mr. A. B. Stavovy - Alternate

LIAISON REPRESENTATIVES

NATIONAL ACADEMY OF SCIENCES-
NATIONAL RESEARCH COUNCIL

Mr. A. R. Lytle - Technical Director, Maritime Transportation Research Board

Mr. R. W. Rumke - Executive Secretary, SRC

AMERICAN IRON AND STEEL INSTITUTE

Mr. J. R. LeCron

BRISTISH NAVY STAFF

Mr. H. E. Hogben
Staff Constructor Officer
Douglas Faulkner, RCNC

WELDING RESEARCH COUNCIL

Mr. K. H. Koopman, Director
Mr. Charles Larson, Secretary

CONTENTS

I. INTRODUCTION

Plastic flow in the locale of notches and cracks has an important bearing on the fracture toughness of alloys(1,2,3)*. Yet the plastic zones attending notches and cracks in heavy sections under tension are not well understood. This is not for lack of interest or attention. The problem has attracted a large number of theoreticians; for example, Allen and Southwell(4), Jacobs(5), McClintock and coworkers(6,7), Prandtl(8), Hill(9), Green(10), Irwin(11), Liu(12), and more recently Bilby and Swinden(13), Tuba(14), and Rice and Rosengren (15) have made important contributions. Although substantial progress has been made--a compilation of slip-line fields and calculated zones is given in Figure 1--the extent of the zone, its shape, and especially, the plastic strain field close to a crack-tip are not established. One reason is that measurements capable of testing the calculations are difficult to make. For example, measurements with strain gages, photoelastic coatings, the interference microscope and moiré grills are: (1) restricted to the specimen surface, (2) do not distinguish between elastic and plastic strain, and (3) do not resolve the steep gradients that characterize the plastic zone in heavy sections.

To circumvent some of these problems the authors adopted Green and Hundy's(17) approach; an etchant was used to reveal the plastic zone, but it was applied to Fe-3Si which responds more sensitively than carbon steel. In the case of Fe-3Si, individual dislocations and slip bands are etched in all grains(18). Thus, even trace amounts of plastic relaxation in regions smaller than the individual grains can be detected at high magnification. In fact, the etching technique appears to be the only method that can sensitively distinguish between elastic and plastic regions. Furthermore, the etching response is graded and can provide information of a quantitative nature for plastic strains up to about 5-10%. Another important advantage is that the etching technique is not restricted to the plate surface but can reveal the plastic zone on interior sections of a plate. The Fe-3Si steel displays stress-strain characteristics similar to those of medium strength ship plate, pressure vessel and constructional steels, and should be a close analogue for these materials. Finally, the results may be applicable to other systems as well since both the Tuba(14) and the Rice and Rosengren(15) theoretical calculations indicate that the size and shape of the plastic zone are relatively insensitive to the rate of strain hardening.

Earlier work on this contract which exploited the etching technique was carried out on relatively thin plates with machined slits (rather than sharp precracks).(19-21) The transition from predominantly in-plane (plane strain) to through-the-thickness (plane stress) relaxation was examined. Preliminary studies of sharp precracks and the effect on the plastic zone of crack growth under load have been reported(3,22,23). Clark(24) has also obtained results on sharp cracks in cantilever beam samples using Fe-3Si steel prepared at Battelle. This report

* See References

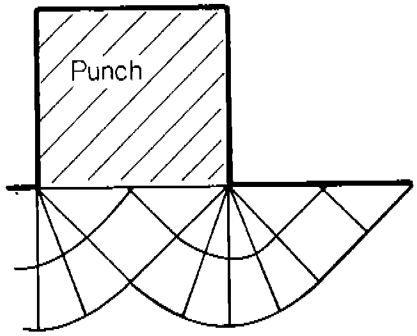

Fig. 1(a) Prandtl - Punch slip-line field.

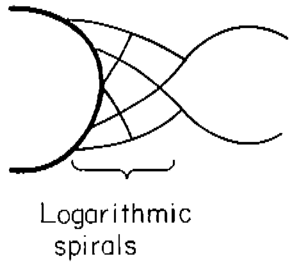

Fig. 1(b) Green-Keyhole Charpy bar slip-line field.

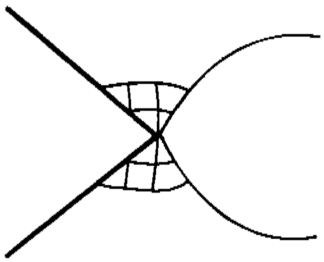

Fig. 1(c) Green-V-notch Charpy bar slip-line field.

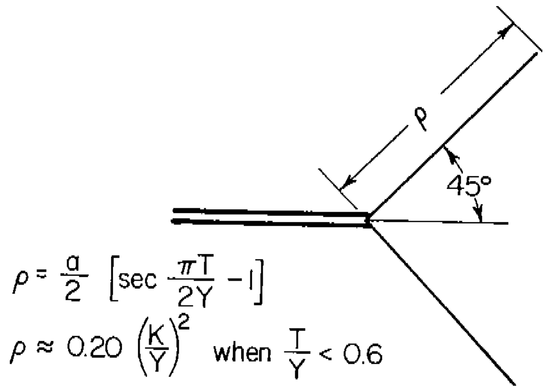

Fig. 1(d) Bilby and Swinden.

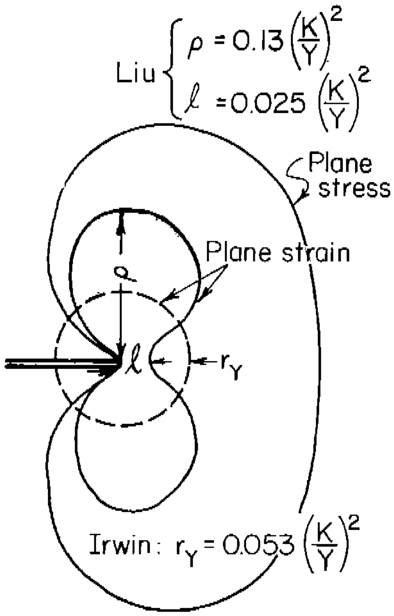

Fig. 1(e) Liu, Irwin-based on elastic stress fields

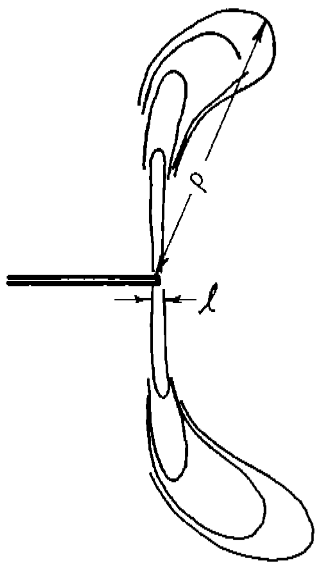

Fig. 1(f) Jacobs.

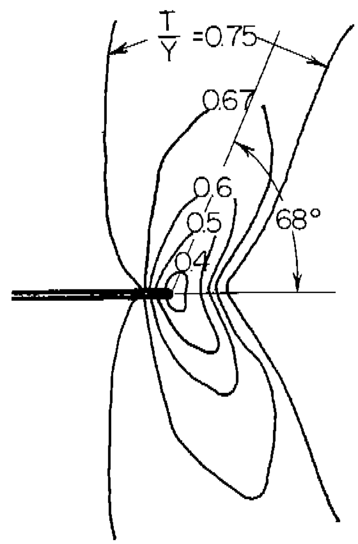

Fig. 1(g) Tuba.

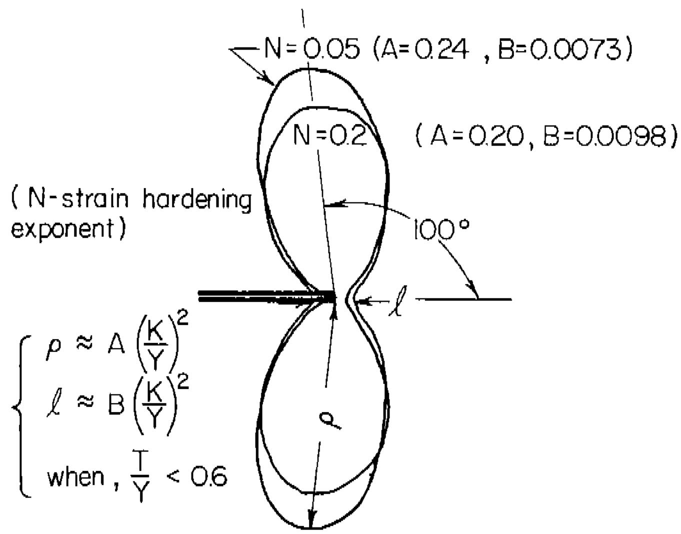

Fig. 1(h) Rice and Rosengren.

Fig. 1. Compilation Of Theoretical Treatments Related To The Plane-Strain, Elastic-Plastic Crack Problem [8 16]

summarizes results for applied stress-crack-length thickness combinations in the range characterized by $0.2 < \left(\frac{K}{Y}\right)^2 \frac{1}{t} < 2$ *. At the lower end of this range the plastic zone is small relative to the plate thickness and in-plane relaxation predominates. Plastic zones generated by edge and center notches, machined slits and sharp pre-cracks were revealed by etching not only the plate surface, but parallel and normal interior sections as well. The etch-figures are augmented by sensitive measurements of the displacements normal to the plate surface existing under load and after the load is removed. Taken together, the work provides a reasonably clear picture of the 3-dimensional character of the strain field in the neighborhood of a crack and allows comparison with theoretical predictions of the size and shape of the plastic zone, and the magnitude of the peak strain.

II. EXPERIMENTAL PROCEDURE

The Fe-3Si steel plates used in this study were obtained from several 100 lb., induction melted heats**, cast, and then upset forged and hot rolled at about 1150 C. The final conversion step was a 50 percent reduction by "warm" rolling at 360 C (to avoid cracking) which leaves the material in a heavily worked condition that recrystallizes on annealing. Prior to machining the test coupons, the rough blanks were stress-relieved for one hour at 475 C to minimize warping. Two types of notches were used: (1) 0.006 in.-wide slits (root radius ~0.003 in.) introduced with a jeweler's saw or abrasive disk, and (2) fatigue cracks grown from 1/8 in.-long slits by cycling in tension between 4,000 psi and 38,000 psi.

After machining, notching, and fatiguing, the test coupons were recrystallized for one hour at 800 C and forced-air-cooled.*** This treatment recrystallizes the material, eliminates dislocations introduced in the warm working operation, by the machining and precracking, and retains in solution carbon and nitrogen needed for decorating the dislocations. The composition and mechanical properties of the different heats in the annealed condition are described in Table 1 and Figure 2(a).

The test coupons, whose dimensions are given in Figure 2, were loaded in an ordinary testing machine via a rod-yoke arrangement that incorporated large spherical bearings to promote alignment. The load was applied at the rate of 4,000 lbs. per minute, held at the predetermined stress level for 4 minutes in the case

---

* For comparison, the ASTM E-24 criterion for plane strain is $\left(\frac{K}{Y}\right)^2 \frac{1}{t} < 0.4$,[25] where $K = T\sqrt{\pi a}$ is the linear elastic fracture mechanics stress intensity parameter, T is the applied stress, Y is the yield stress, and t is the plate thickness.

** Melted from a charge of Armco iron and Fe-Si with about 0.03 percent nickel added as a deoxidizer.

*** Heating in air with the coupons wrapped in steel foil produced a tarnished surface but detracted less from the etching response of material close to the surface than treatments in commercial vacuum furnaces. Samples given a prolonged furnace cool did not etch.

TABLE 1. COMPOSITION AND PROPERTIES OF FE-3Si STEEL[a]

Heat	Composition (wt%) Si	C	N	Lower Yield Stress[b] (psi)	Other Mechanical Properties (Room Temp)
S	3.26	0.015	0.001	62,000/64,000	
X	3.45	0.009	<0.001	62,000	
FF	3.39	0.012	0.001	59,000	
GG	3.40	0.013	0.001	64,000	Upper yield: 66,000 psi, Lüders strain 0.5-1.5%, ultimate: 83,000 psi, true fracture stress: 140,000 psi, true fracture strain: 0.9-1.2 (fibrous mode), strain hardening exponent in strain hardening region: N = 0.16

(a) Annealed condition

(b) Measured at a strain rate of 3.10^{-4} to 3.10^{-5} sec^{-1} .

of the slits and 4 seconds for the sharp precracks, and then unloaded at the same rate. The loads are alternatively expressed in terms of the nominal (gross section) stress T, the nominal stress to (lower) yield stress ratio $\frac{T}{Y}$, and as the stress intensity parameter $K \equiv T\varphi\sqrt{\pi a}$. Here, a is the length of an edge crack or the half-length of a center crack, and φ is a correction for the width of the sample* (φ = 1.12 for an 0.25 in.-long edge crack in a 2.5 in.-wide sample).[26] Changes in the thickness of the coupons in the region close to the crack tip were measured in two ways. In one case a series of plastic replicas of the plate surface was made at different load levels; the contours of the replicas were then charted with a surface profile device. This technique, which has a sensitivity of about 10^{-5} in., is described more fully in Reference 21. In the second case the residual displacements normal to the plate surface were measured after unloading with an interference microscope[19,27].

After the coupons were loaded, they were aged at 150 C for twenty minutes to decorate the dislocations generated by plastic flow thereby sensitizing them to the etchant. Any cold work introduced after aging in the course of sectioning and hand polishing is not 'decorated' and not attacked by the etchant.** One complication is that machine grinding and abrasive cut-off wheels tend to produce a heavily disturbed surface layer 0.005 to 0.010 in.-thick which does not respond to etching under any conditions; this layer must be removed by gentle hand grinding with metallurgical paper to obtain satisfactory etching responses.

* The elastic correction of Isida, reported in Reference (26), was used. An elastic-plastic correction that takes into account the boundary conditions on the loaded edges of the specimen is now being worked out at Battelle and will appear in the forthcoming Annual Report on Air Force Contract No. AF33(615)-3565.

** Note that decoration will occur after prolonged periods at room temperature or if the sample becomes hot during machining and grinding.

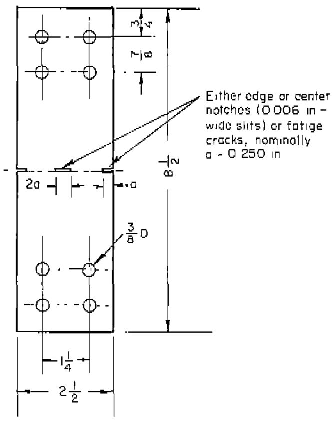

Fig. 2(a).

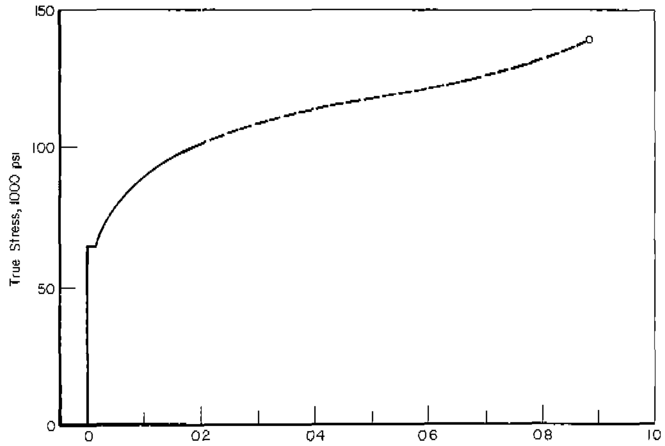

Fig. 2(b) True Plastic Strain.

Fig. 2 TEST COUPONS AND MECHANICAL PROPERTIES: (a) configuration of test coupons and (b) example of the true stress-true strain properties of heat GG.

The Fe-3Si samples were electropolished and etched in the Morris solution(29).*** The etching characteristics of the Fe-3Si steel is illustrated in Figures 3 and 4. When the annealed material is strained plastically small amounts, i.e., 0-0.5%, etching reveals individual dislocations and slip bands. Strains in the range 0.5 to 5% produce so many dislocations that the individual pits can no longer be resolved in the light microscope; etching merely darkens the surface in this range. Beyond 5 to 7%, the air-cooled material stops etching presumably because there is insufficient carbon and nitrogen in solution for decoration.(30) In this way the etching response can provide an approximate quantitative indication of the local strain intensity. For example, the existence of an unetched region surrounded by a dark etching material around a strain concentration is indicative of a peak strain in excess of about 5-7%. Figure 5 shows that the strain corresponding

---

*** Composition of the electrolyte: 7 cc H_2O, 25 gm chromium trioxide, 133 cc glacial acetic acid. Polishing occurs in the range 22-40 volts with a stainless steel cathode and specimen-cathode separation of 1/4-3/4 in., in 5-20 minutes with the solution agitated and maintained at 20 C. Etching occurs at about 5 volts in 3-15 minutes without agitation.

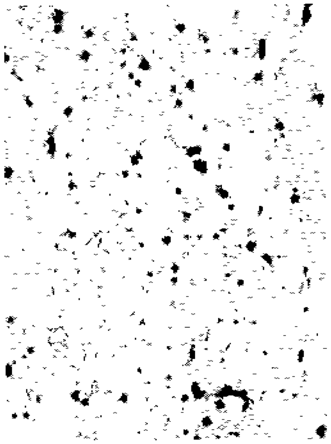

Fig. 3(a) $\varepsilon_p = 0.$

Fig. 3(b) Stressed 0.09Y.

Fig. 3(c) $\varepsilon_p = 0.01.$

Fig. 3(d) $\varepsilon_p = 0.015.$

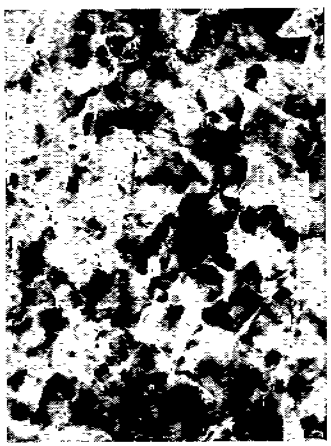

Fig. 3(e) $\varepsilon_p = 0.03.$

Fig. 3(f) $\varepsilon_p = 0.05.$

Fig. 3(g) $\varepsilon_p = 0.07.$

Fig. 3(h) $\varepsilon_p = 0.10.$

Fig. 3 ETCHING RESPONSE OF UNNOTCHED Fe-3Si (HEAT S) TENSILE BARS STRAINED DIFFERENT AMOUNTS. The bars were annealed at 800 C and air-cooled except the one shown in Figure (c) which was annealed at 1200 C to eliminate discontinuous yielding so as to obtain a uniform strain of 0.01%. ε_p is the plastic strain. 54X


Fig. 4(a) $\varepsilon_p = 0.01$.


Fig. 4(b) $\varepsilon_p = 0.04$.

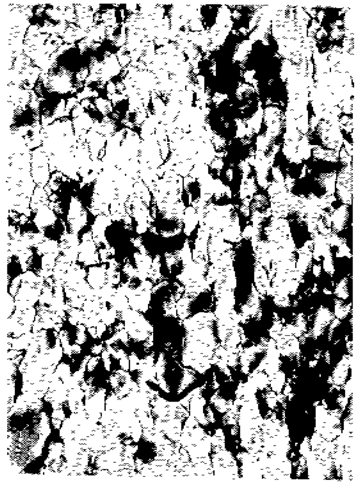
Fig. 4(c) $\varepsilon_p = 0.07$.

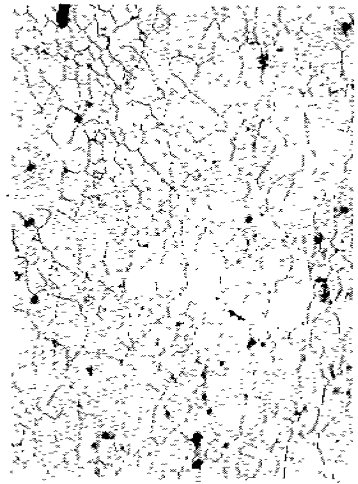
Fig. 4(d) $\varepsilon_p = 0.12$.


Fig. 4(e) $\varepsilon_p = 0.01$.


Fig. 4(f) $\varepsilon_p = 0.03$.

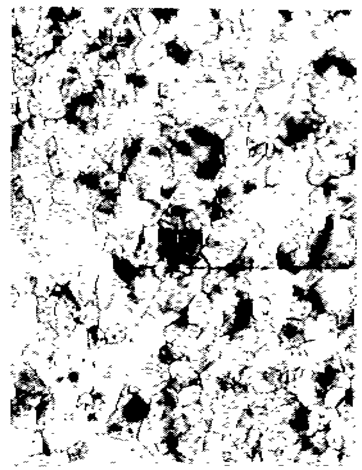
Fig. 4(g) $\varepsilon_p = 0.07$.

Fig. 4 ETCHING RESPONSE OF UNNOTCHED Fe-3Si (HEAT GG) TEST BARS STRAINED DIFFERENT AMOUNTS: (a)-(d) deformed in tension, and (e)-(g) deformed in compression. ε_p *is the plastic strain.* **90X**

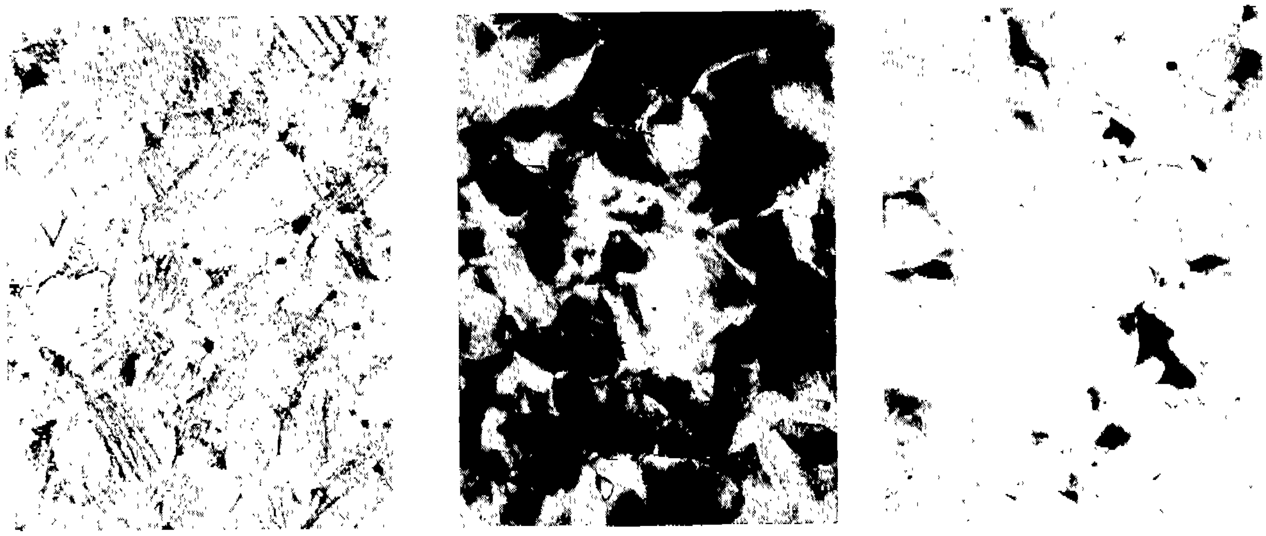

Fig. 5(a) $\varepsilon_p = 0.$ *Fig. 5(b)* $\varepsilon_p = 0.10.$ *Fig. 5(c)* $\varepsilon_p = 0.15.$

Fig. 5 ETCHING RESPONSE OF UNNOTCHED Fe-3Si (HEAT S) TENSILE BARS STRAINED DIFFERENT AMOUNTS. These bars were water-quenched from the 800 C annealing temperature. ε_p *is the plastic strain. 135X*

to the loss of etching response can be increased from 5-7% to 10-15% by water quenching, but this has the disadvantage of introducing quenching strains which are also revealed by the etchant. Figure 4 illustrates that plastic deformation produced by tension and by compression etch in the same way.

III. EXPERIMENTAL RESULTS

The experimental results are summarized in Tables 2 and 3, and are set forth in more detail in Figures 6-23. Several complications that affect their interpretation should be noted at the outset:

1. Not all grains are recrystallized; isolated grains undergo a recovery process and these are filled with a dense substructure that etches darkly in the absence of plastic deformation* (examples can be seen in Figures 18, 21, and 23).

2. Plastic deformation during loading is followed by reverse deformation during unloading, at least close to the crack tip[6,31]. The present etching procedure does not separate these two components**.

(Manuscript continued on page 40)

* Such grains are undesirable because they can obscure the plastic zone. However, their presence does not perturb the plastic zone, and this indicates that the recovered grains are not significantly stronger than recrystallized grains.

** An attempt was made to separate the two deformations by aging the sample under load (80% of full load) and cooling them before unloading, thus rendering the reverse deformation transparent to the etchant. However, this procedure produced fuzzy, ill-deformed zones--evidently the samples creep at the aging temperature--and was abandoned.

TABLE 2. SUMMARY OF TEST DATA

(a) Sample No.	Thickness (in)	(b) Notch Geometry	(c) T (ksi)	(d) $\frac{T}{Y}$	(e) K (ksi$\sqrt{\text{in}}$)	(f) $\frac{K}{Y}$ ($\sqrt{\text{in}}$)	(g) Zone Extent, ρ (in)	(h) Zone Width, ℓ (in)	$\frac{2\rho}{t}$	$\left(\frac{K}{Y}\right)^2 \frac{1}{t}$
S-52	0.195	0.25 (M) EN	12.8	0.21	12.8	0.21	0.010	-	0.1	0.23
S-118	0.199	0.25 (M) EN	19.8	0.31	19.8	0.31	0.025	0.010	0.4	0.48
S-57	0.196	0.25 (M) EN	26.3	0.42	26.3	0.42	0.055	0.010	0.55	0.90
X-2	0.428	0.25 (M) EN	27.3	0.42	27.5	0.42	0.060	0.015	0.21	0.41
S-117	0.198	0.25 (M) EN	29.8	0.46	29.8	0.46	0.075	0.015	0.06	1.07
S-60	0.195	0.25 (M) EN	40.0	0.64	40.0	0.64	> 0.5 (i)	0.020	> 5	2.10
S-101	0.019	0.38 (F) EN	9.4	0.15	11.4	0.18	0.010	0.003	1	1.70
S-107	0.058	0.25 (F) EN	13.4	0.21	13.4	0.21	0.010	0.003	.35	0.76
GG-6	0.220	0.22 (F) EN	22.6	0.35	21.0	0.33	0.010	0.003	0.09	0.50
X-47	0.420	0.22 (F) CN	25.2	0.41	23.4	0.38	0.040	0.004	0.2	0.34
FF-3	0.212	0.25 (F) EN	22.2	0.38	22.2	0.38	0.040	0.008	0.4	0.68
X-49	0.420	0.22 (F) EN	27.2	0.43	25.2	0.41	0.030	0.003	0.15	0.40
FF-8	0.212	0.25 (F) CN	30.7	0.52	27.2	0.46	0.070	0.010	0.65	1.00
GG-5	0.220	0.22 (F) EN	33.0	0.51	30.7	0.48	0.050	0.006	0.45	1.05
X-46	0.420	0.30 (F) CN	25.3	0.57	35.8	0.58	0.230	0.010	1.1	0.80
X-50	0.420	0.22 (F) EN	48.0	0.77	45.2	0.73	> 0.5 (i)	-	> 2	1.27

(a) Letter preceding number designates heat number.
(b) Number gives slit or crack length (half length for center crack); (F) designates fatigue crack, (M) machined slit, 0.006 in. wide; EN - edge notch, CN - center notch
(c) T is the gross section stress, (d) Ratio of gross section stress to lower yield stress.
(e) $K \equiv T\varphi\sqrt{\pi a}$, where T is gross section stress, a is edge crack length (center half-length) and φ is the correction for free surface.[26]
(f) Ratio of stress intensity to lower yield stress.
(g) Distance between crack tip (or slit free surface) and furthest extent of plastic deformation measured radially from crack tip (or from a point on the center line of the slit and 0.003 in. from the center of curvature of the slit tip).
(h) Width of the zone of in-plane shear at the crack tip.
(i) Plastic zones from opposite edge notches merge.

TABLE 3. STRAINS AND DISPLACEMENTS AT THE CRACK TIP ARISING FROM THROUGH-THE-THICKNESS PLASTIC DEFORMATION

Sample	t (in)	$\frac{K}{Y}$ ($\sqrt{in}$)	$\left(\frac{K}{Y}\right)^2 \frac{1}{t}$	(a) w (10^{-5} in.) Under Load	(a) w (10^{-5} in.) After Unloading	(b) $\bar{\epsilon}_z$ Under Load	(b) $\bar{\epsilon}_z$ After Unloading	(d) v_c' (10^{-5} in.) Under Load	(d) v_c' (10^{-5} in.) After Unloading	(e) v_c'' (10^{-5} in.) Under Load	$\frac{v_c'}{v_c''}$ Under Load
X-3	0.420	0.48	0.55	-30	-	- 0.0014	-	2.6	-	13.8	0.19
		0.56	0.75	-40	-	- 0.0019	-	3.8	-	19.4	0.20
		0.64	1.04	-57	-	- 0.0027	-	8.1	-	27.1	0.30
		0.72	1.24	-95	-	- 0.0045	-	18.7	-	37.0	0.50
X-2	0.428	0.42	0.41	-	-10	-(0.0010) (c)	-0.0005	~(2.6) (c)	1.3	10.1	0.26
S-118	0.199	0.31	0.48	-	- 5	-(0.0010) (c)	-0.0005	~(1.6) (c)	0.8	5.3	0.30
S-107	0.058	0.21	0.76	-	- 5	-(0.0034) (c)	-0.0017	~(0.4) (c)	0.2	2.4	0.20
S-57	0.196	0.42	0.90	-	-10	-(0.0020) (c)	-0.0010	~ (3.80) (c)	1.9	10.1	0.38
S-117	0.198	0.46	1.07	-	-14	-(0.0028) (c)	-0.0014	~ (7.00) (c)	3.5	12.4	0.57
S-101	0.019	0.18	1.70	-	- 4	-(0.0084) (c)	-0.0042	~(15.6) (c)	7.3	1.7	9.10
S-60	0.195	0.64	2.10	-	-36	-(0.0074) (c)	-0.0037	~(30.0) (c)	15.0	27.1	1.10
S-58	0.232	0.72	2.25	-	-60	-(0.0104) (c)	-0.0052	~ (53.4) (c)	26.7	37.0	1.45

(a) w is the maximum z-direction displacement of the plate surface produced by plastic through-the-thickness deformation. Values quoted are the displacement of a point 1-mill from the crack tip relative to a point just outside the plastic zone, e.g., points (1) and (2) in Figure 12(b). These displacements under load were derived from plastic replicas of the surface taken under load. Residual displacements were obtained from interferometric patterns of the surface as shown in Figure 12.

(b) $\bar{\epsilon}_z \cong \frac{2w}{t}$, where t is the plate thickness. $\bar{\epsilon}_z$ is the average strain at the crack tip.

(c) Estimated as follows: $\bar{\epsilon}_z$ (under load) = $2\bar{\epsilon}_z$ (after unloading), or v_c' (under load) = $2v_c'$ (after unloading)

(d) v_c' is the component of the crack opening (y-direction) displacement at the crack (or slit) tip produced by through-the-thickness ($\gamma_{yz,yz}$- and $\gamma_{xy,yz}$) relaxations: values quoted were calculated: $v_c' = -\frac{1}{t}\int_{y=0}^{y=\infty} w\,dy$

(e) v_c'' is the component of crack opening (y-direction) displacement at the crack (or slit) tip produced by in-plane ($\gamma_{xy,xy}$) relaxations. Values quoted are estimates based on the Bilby-Swinden[13] model: $v_c'' = \frac{2Ya}{\pi E} \ln \sec \frac{\pi T}{2Y}$.

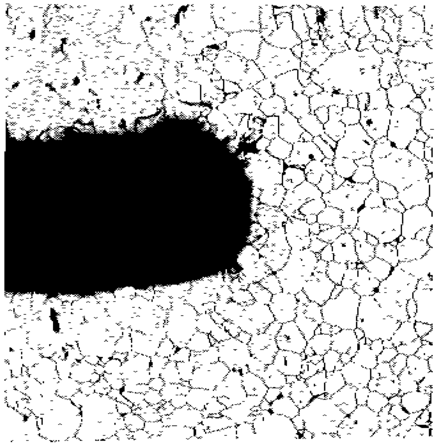

Fig. 6(a) Plate Surface.

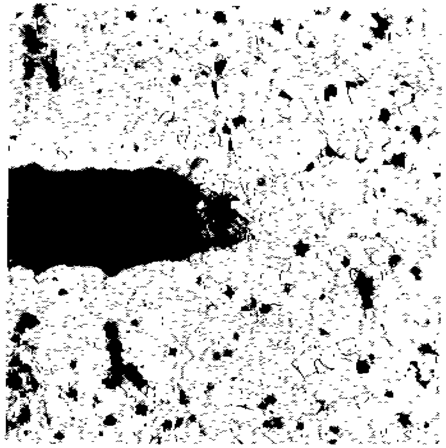

Fig. 6(b) Intermediate Section.

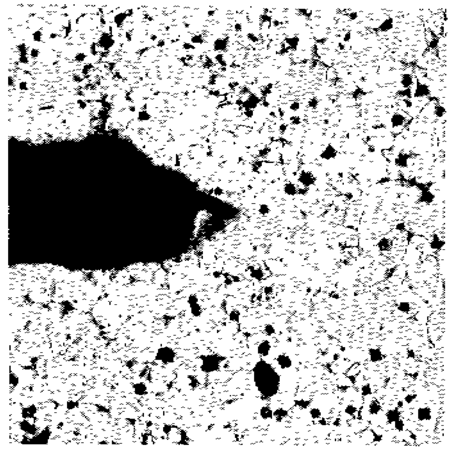

Fig. 6(c) Plate Midsection.

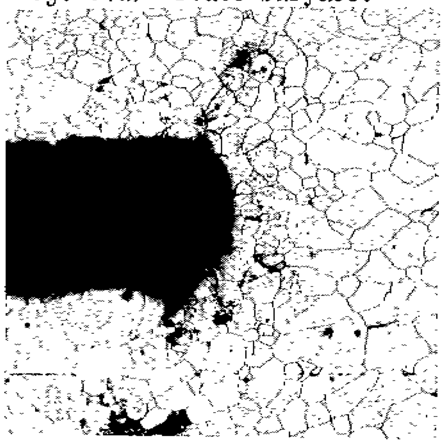

Fig. 6(d) Plate Surface.

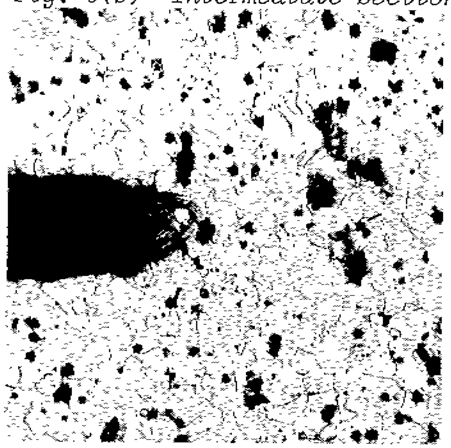

Fig. 6(e) Intermediate Section.

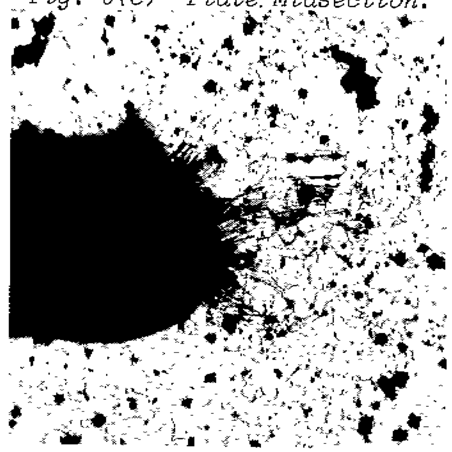

Fig. 6(f) Plate Midsection.

Fig. 6 PLASTIC ZONES DISPLAYED BY SAMPLE S-52 ($t = 0.195$, $\frac{K}{Y} = 0.21\ \sqrt{in}$) ON THE PLATE SURFACE AND ON INTERIOR SECTIONS PARALLEL TO THE SURFACE: (a), (b) and (c) represent an edge slit; (d), (e), and (f) the other slit. 54X

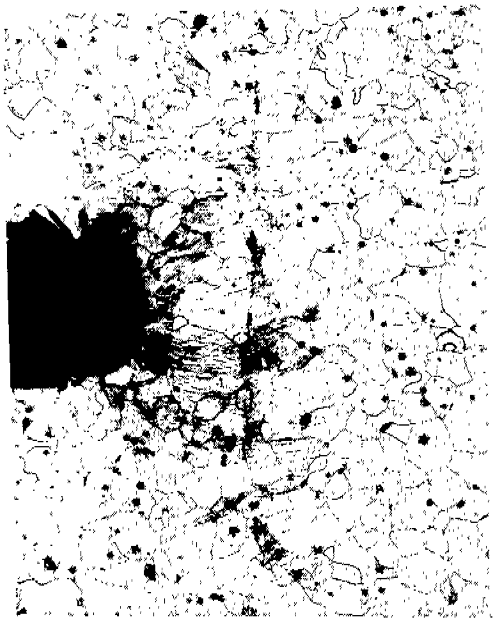

Fig. 7(a) Plate Surface.

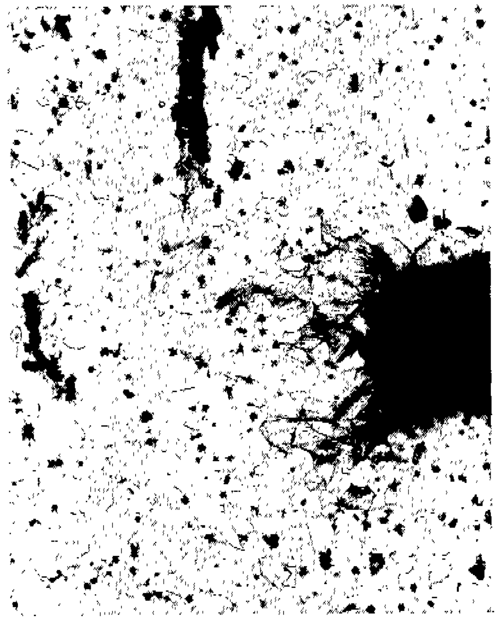

Fig. 7(c) Plate Surface.

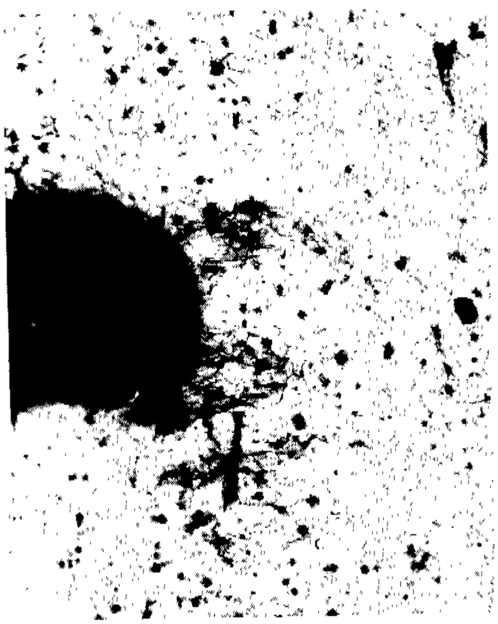

Fig. 7(b) Plate Surface.

Fig. 7(d) Plate Midsection.

Fig. 7 PLASTIC ZONES DISPLAYED BY SAMPLE S-118 ($t = 0.199$, $\frac{K}{Y} = 0.31 \sqrt{in}$): (a) and (b) show sections of the two edge slits close to one of the plate surfaces, (b) is the same notch as (a) on the opposite face, (d) is the plate midsection intermediate between (a) and (b), and (e) is the same zone as (d). (a)-(d) are 60X, (e) is 180X

Fig. 7(e) Plate Midsection.

Fig. 7 PLASTIC ZONES DISPLAYED BY SAMPLE S-118. *(Continued)*

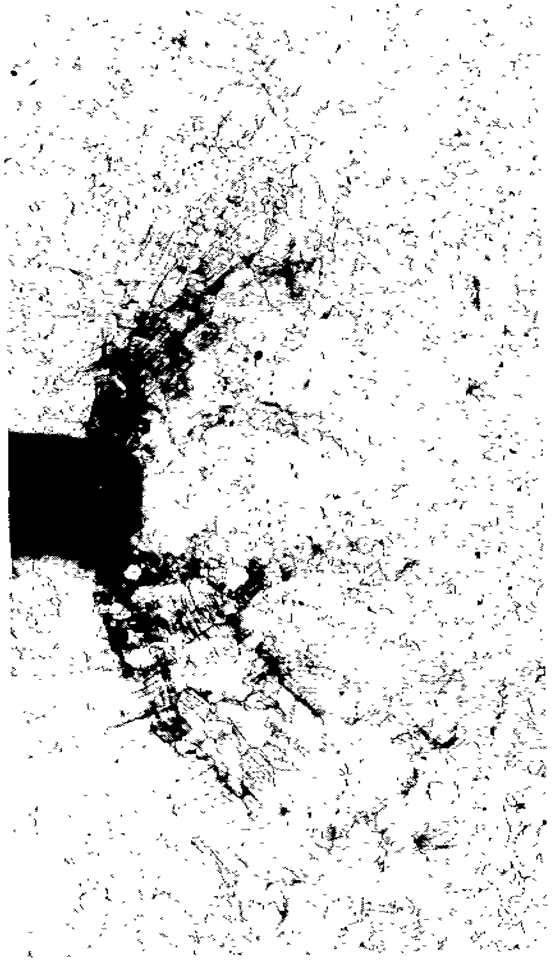

Fig. 8(a) Plate Surface.

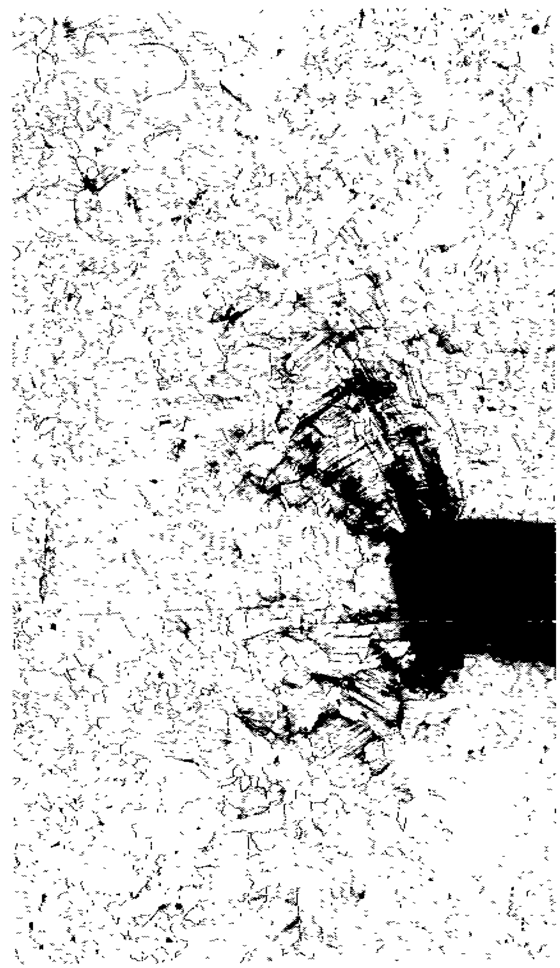

Fig. 8(b) Plate Surface.

Fig. 8 PLASTIC ZONES DISPLAYED BY SAMPLE S-57 ($t = 0.196$ in, $\frac{K}{Y} = 0.42$ in): (a) and (b) show the zones produced by the two edge-slits near the surface of one side of the plate, (c) shows the same slit as (a) on the opposite side of the plate close to the plate surface, (d) and (e) are parallel to (c); (d) half-way between the surface and the midsection, and (e) is the plate midsection. 36X

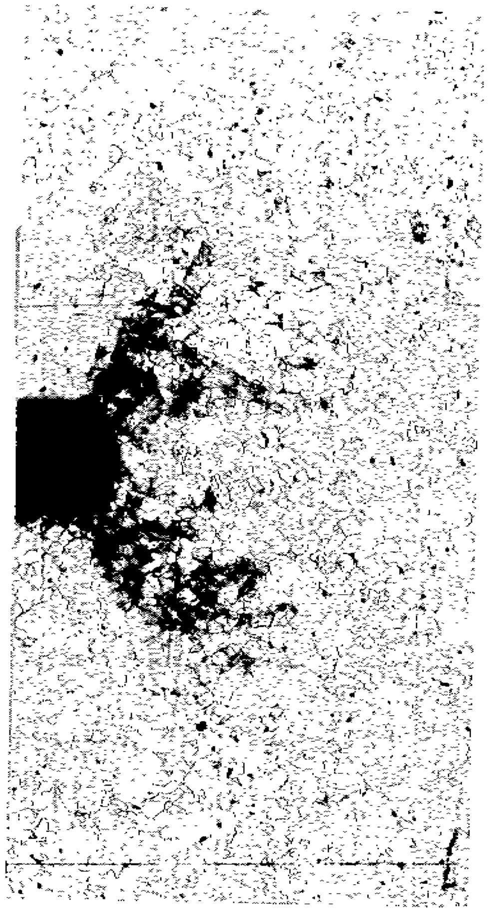

Fig. 8(c) Plate Surface.

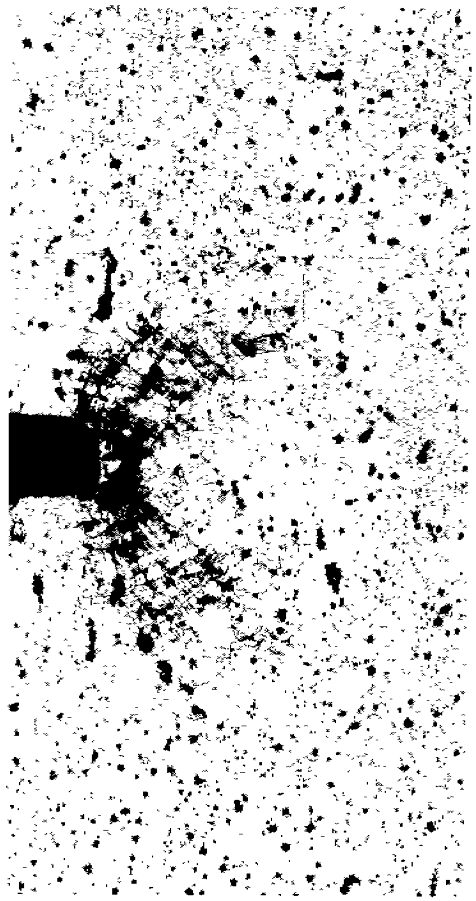

Fig. 8(d) Intermediate Section.

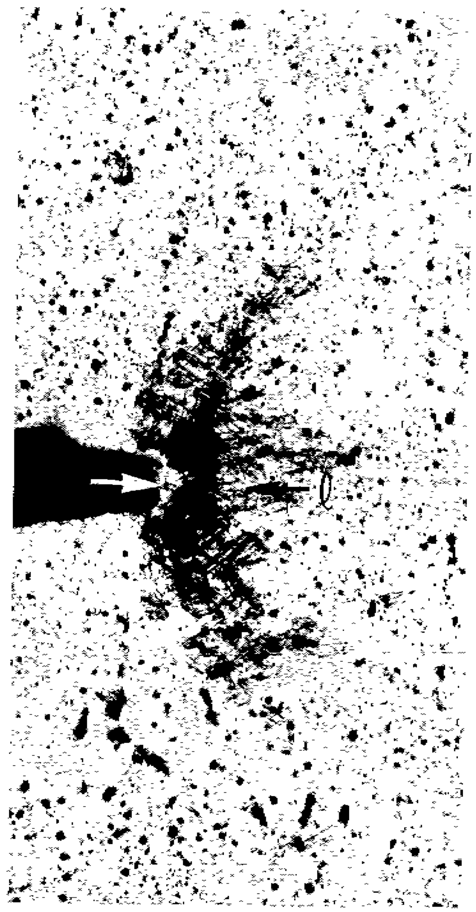

Fig. 8(e) Plate midsection.

Fig. 8 PLASTIC ZONES DISPLAYED BY SAMPLE S-57 (Continued)

Fig. 9(b) Section 11.

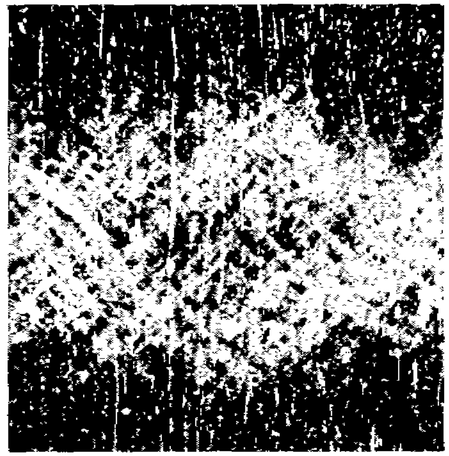

Fig. 9(c) Section 22.

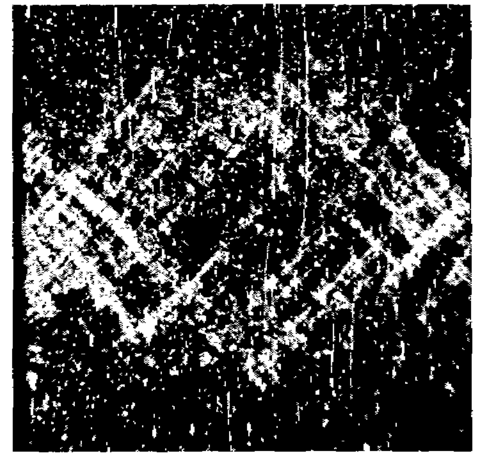

Fig. 9(d) Section 33

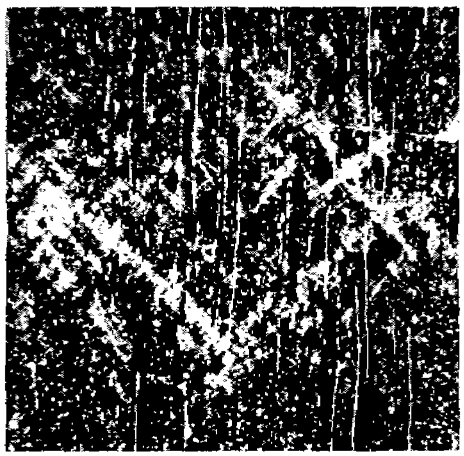

Fig. 9(e) Section 44.

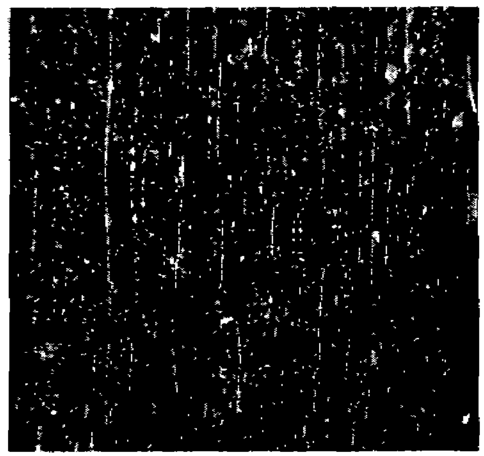

Fig. 9(f) Section 55.

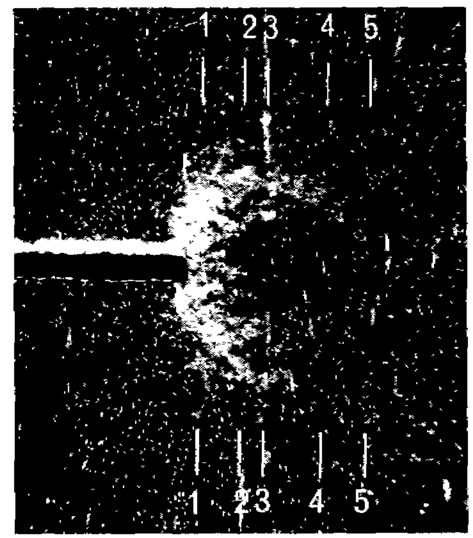

Fig. 9(a) Plate Surface.

Fig. 9 PLASTIC ZONE DISPLAYED BY SAMPLE S-117 (t = 0.198 in, $\frac{K}{Y}$ = 0.46 $\sqrt{in}$): (a) section close to and parallel to the plate surface, and (b)-(f) sections normal to the plate surface and the slit plane, (g) same as (a) at higher magnification. (a)-(f): oblique illumination, 13.5X; (e) 54X

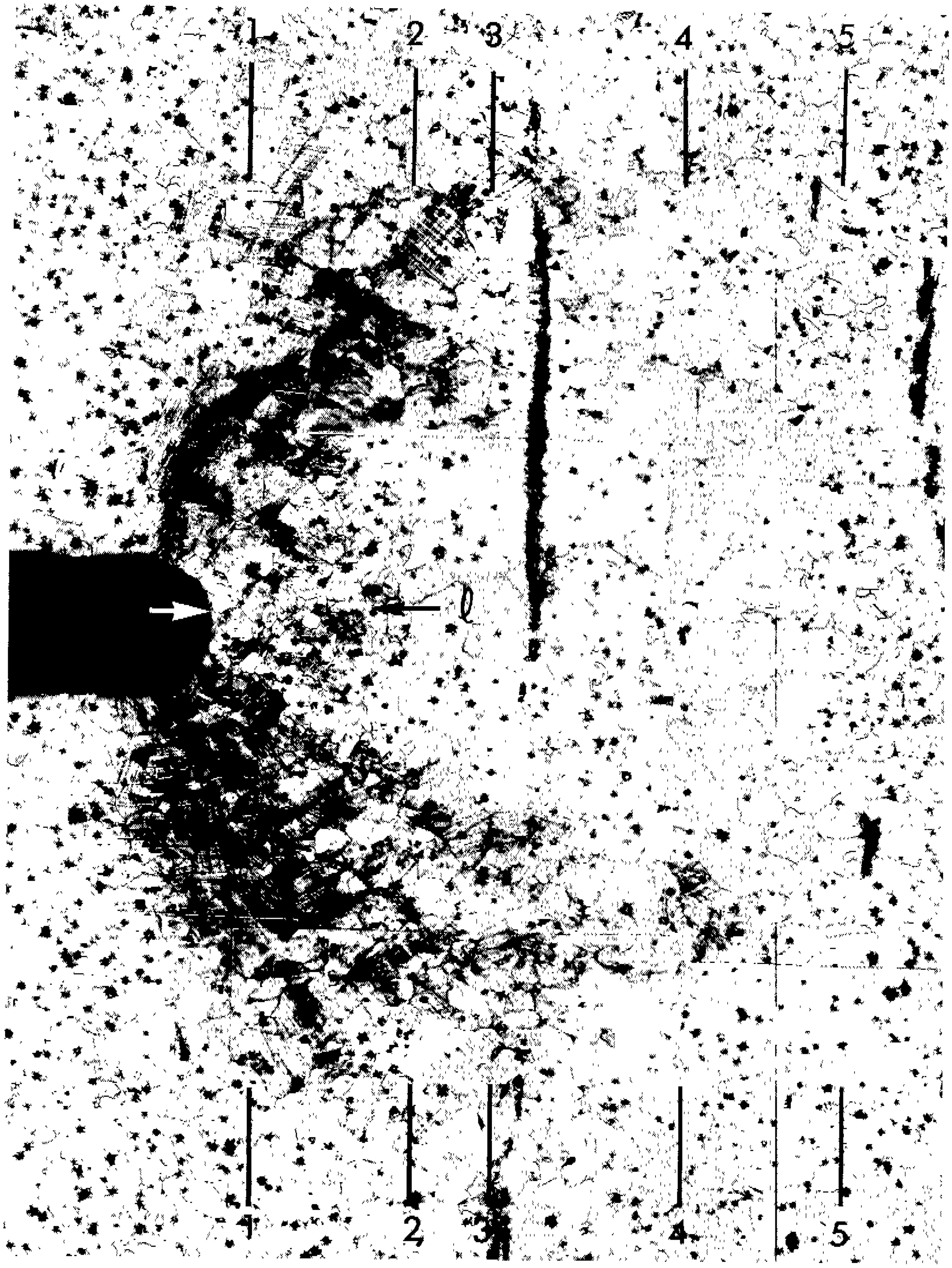

Fig. 9(g) Plate Surface.

Fig. 9 PLASTIC ZONE DISPLAYED BY SAMPLE S-117 (Continued)

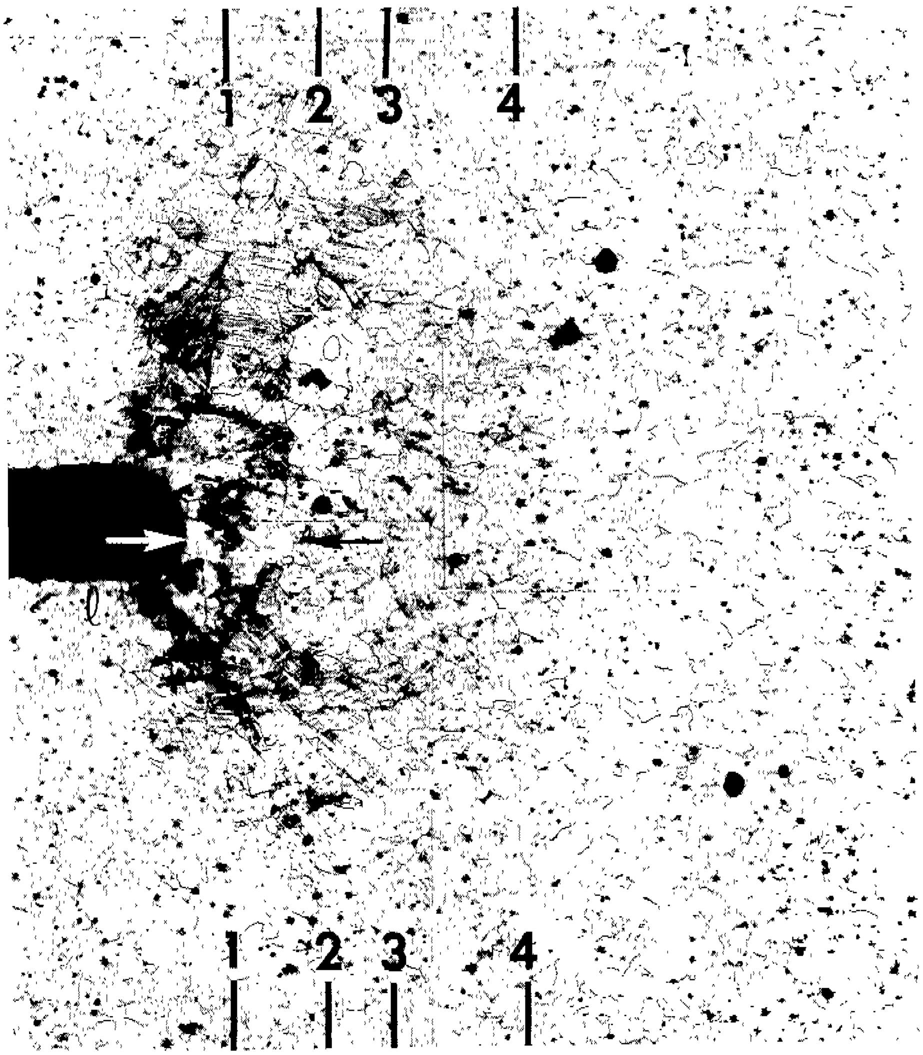

Fig. 10(a) Plate Surface.

Fig. 10. PLASTIC ZONE DISPLAYED BY SAMPLE X-2 ($t = 0.406$, $\frac{K}{Y} = 0.42\sqrt{in}$): (a) Section Close to and Parallel to the Plate Surface, 64X, and (b)-(e) Sections Normal To The Plate Surface and the Slit Front, 12X

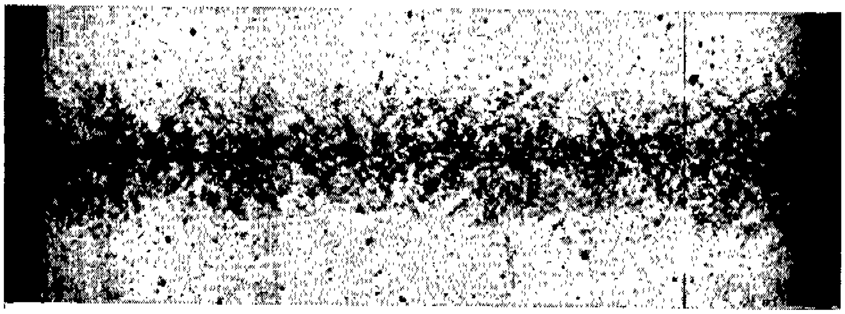

Fig. 10(b) Section 11.

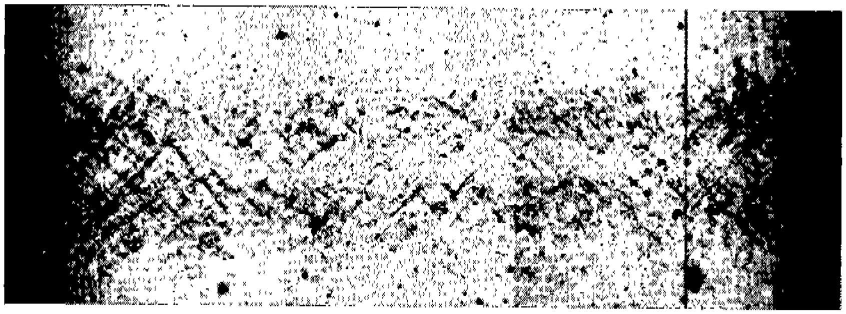

Fig. 10(c) Section 22.

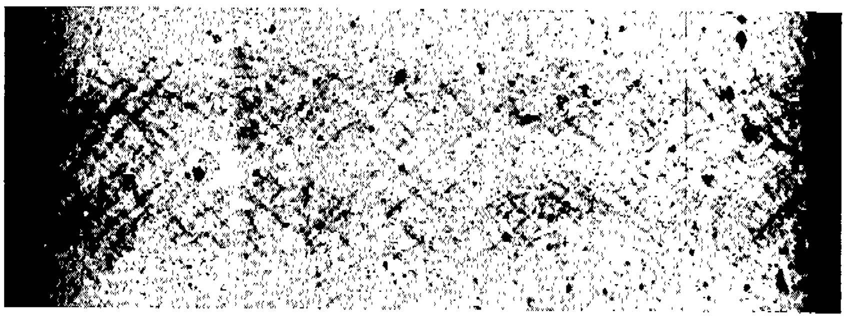

Fig. 10(d) Section 33.

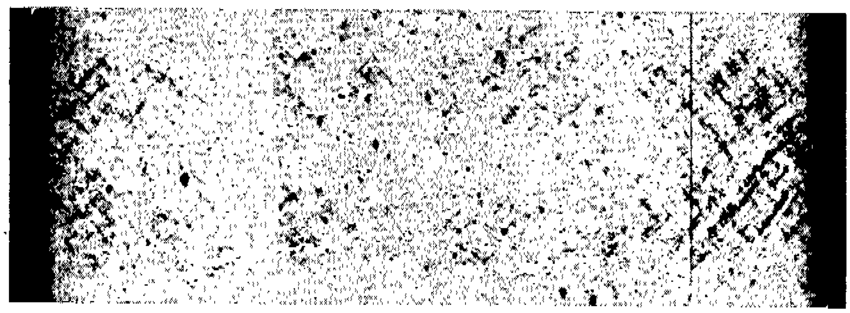

Fig. 10(e) Section 44.

Fig. 10 PLASTIC ZONE DISPLAYED BY SAMPLE X-2. (continued)

Fig. 11(a) Surface.

Fig. 11 PLASTIC ZONES DISPLAYED BY SAMPLE S-60 ($t = 0.195$ in, $\frac{K}{Y} = 0.64 \sqrt{in}$) ON SECTIONS PARALLEL TO THE PLATE SURFACE: (a) close to plate surface, (b) half-way between plate surface and midsection, and (c) plate midsection. 22X

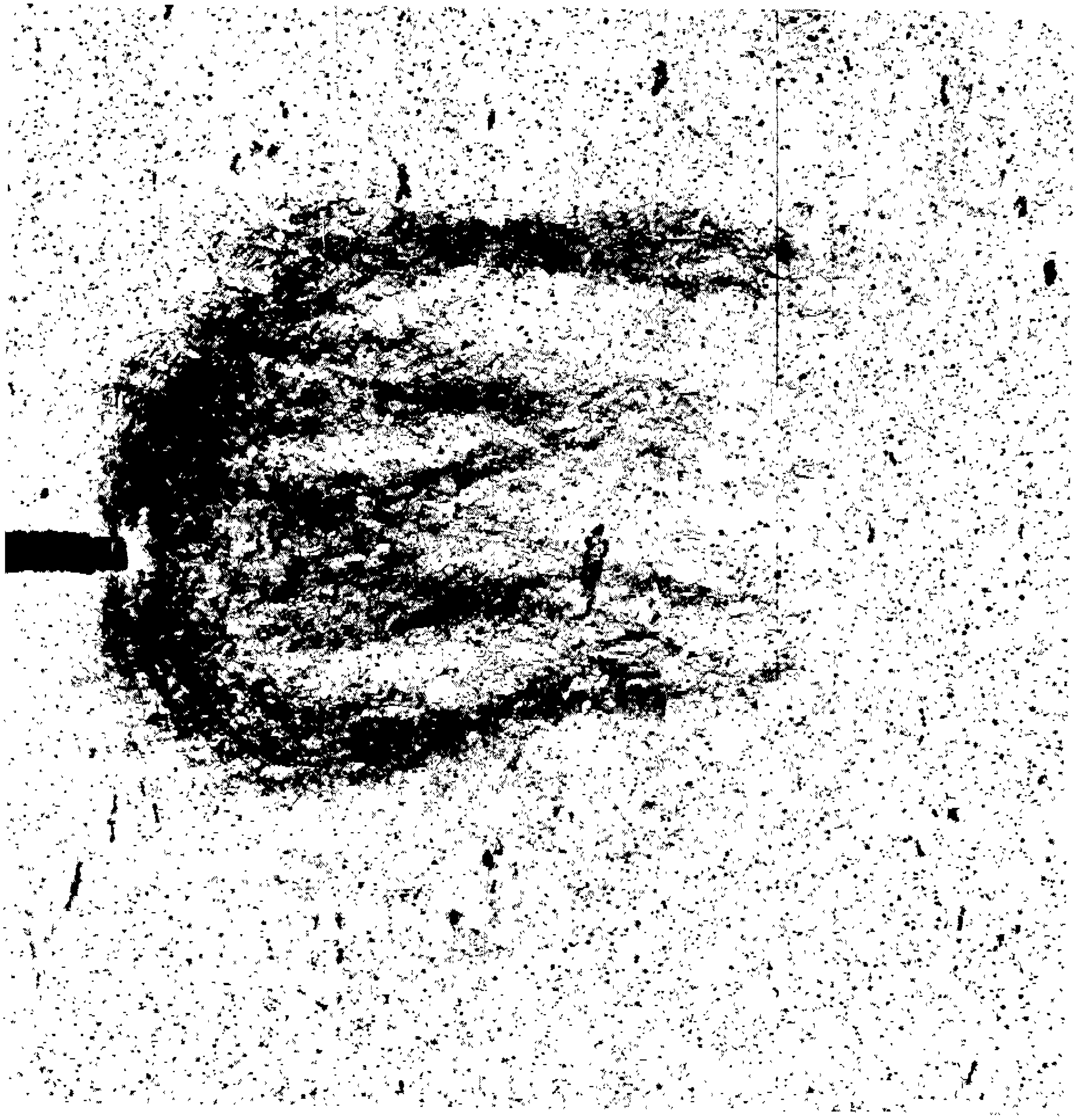

Fig. 11(b) Intermediate Section.

Fig. 11 PLASTIC ZONES DISPLAYED BY SAMPLE S-60 (Continued)

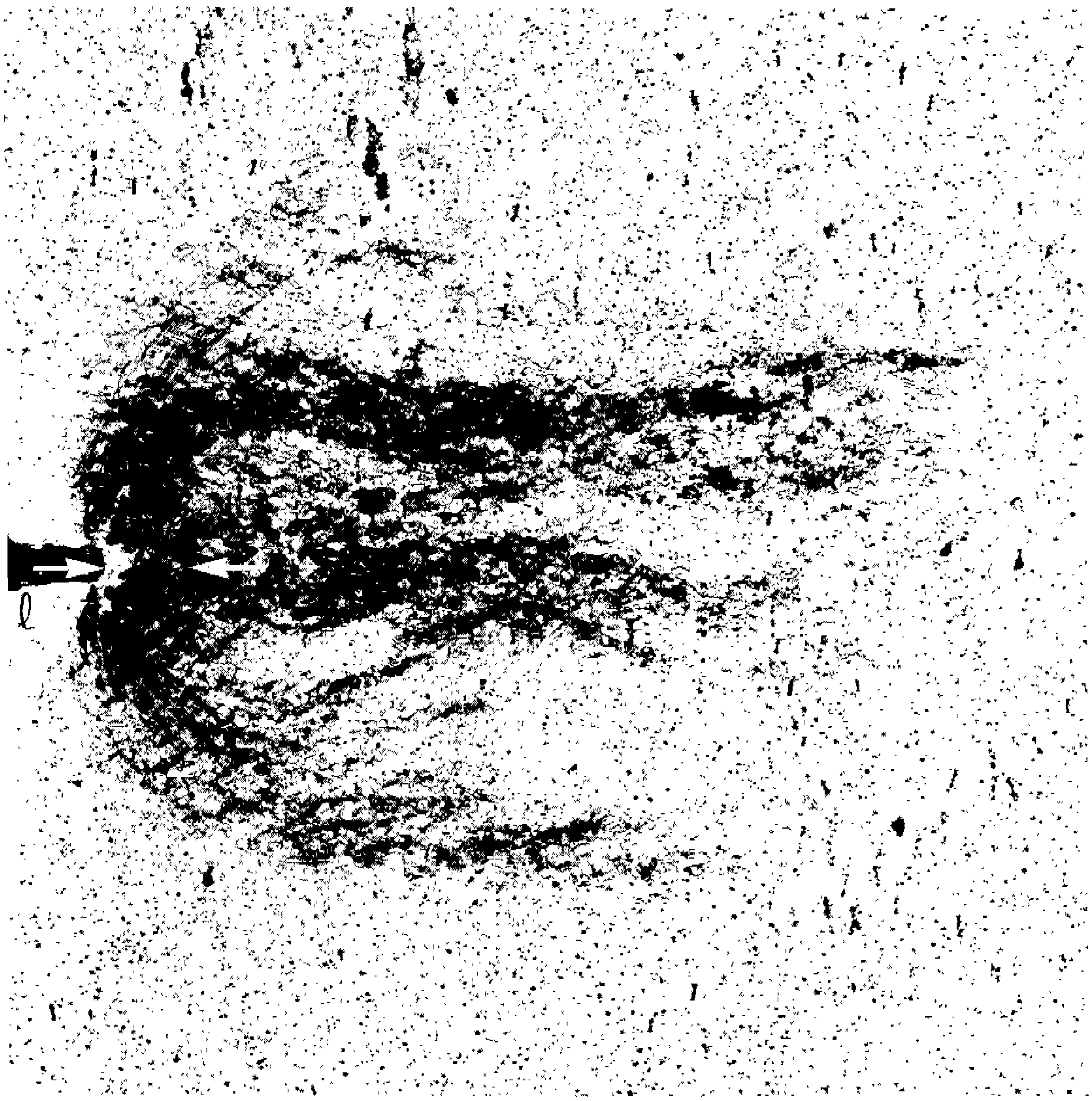

Fig. 11(c) Midsection.

Fig. 11 PLASTIC ZONES DISPLAYED BY SAMPLE S-60. (Continued)

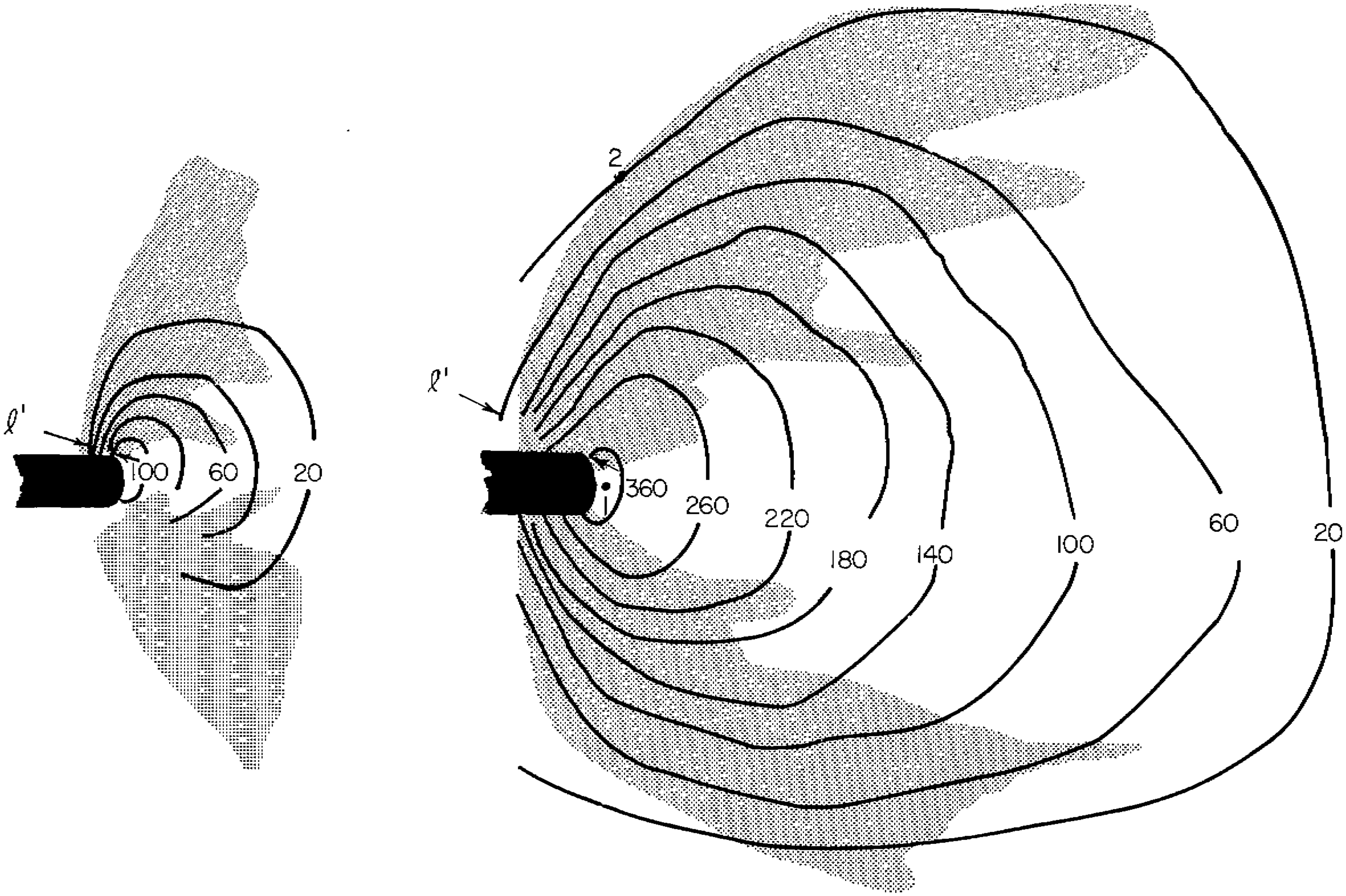

(a)

(b)

Fig. 12(e)

Fig. 12(b)

Fig. 12 SURFACE DISPLACEMENT CONTOURS DERIVED FROM INTERFEROMETRIC FRINGE PATTERNS: (a) sample S-57 ($\frac{K}{Y}$ = 0.42 $\sqrt{in.}$), and (b) sample S-60 ($\frac{K}{Y}$ = 0.64 $\sqrt{in.}$). The numbers assigned to the contours are the (negative) displacements in microinches. The contours coincide with the plastically deformed regions (shaded areas) revealed on the surface by etching. 22X

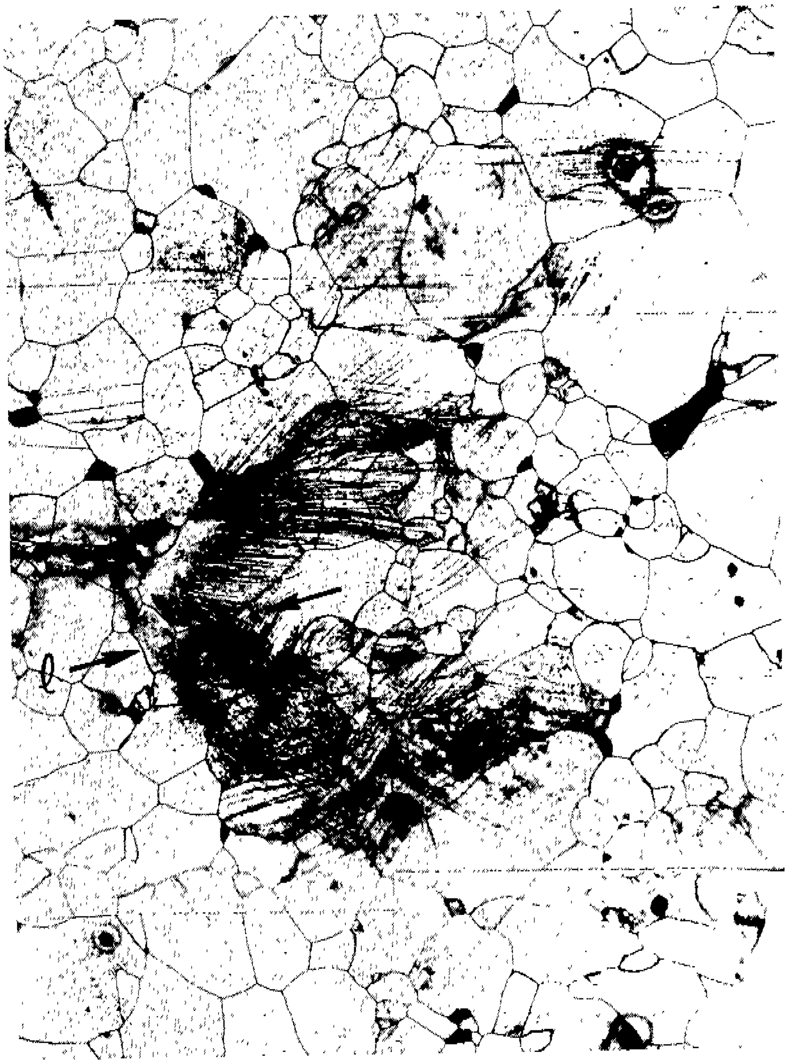

Fig. 13 PLASTIC ZONES DISPLAYED BY SAMPLE S-101 ($t = 0.019$ in, $\frac{K}{Y} = 0.18 \sqrt{in}$) NEAR THE PLATE SURFACE.

Fig. 14 (a) Plate Surface.

Fig. 14(b) Plate Surface.

Fig. 14 PLASTIC ZONES DISPLAYED BY SAMPLE S-107 (t = 0.058 in, $\frac{K}{Y} = 0.21 \sqrt{in}$): (a) and (b) show the zones of the two edge cracks as they appear in sections close to and parallel to the surface on one side of the plate, 180X, (c) is a view of the crack shown in (a) from the opposite side of the plate, 54X (d) is a portion of (c) at 180X, and (e)-(i) are sections normal to the plate surface (54X) identified in (a)

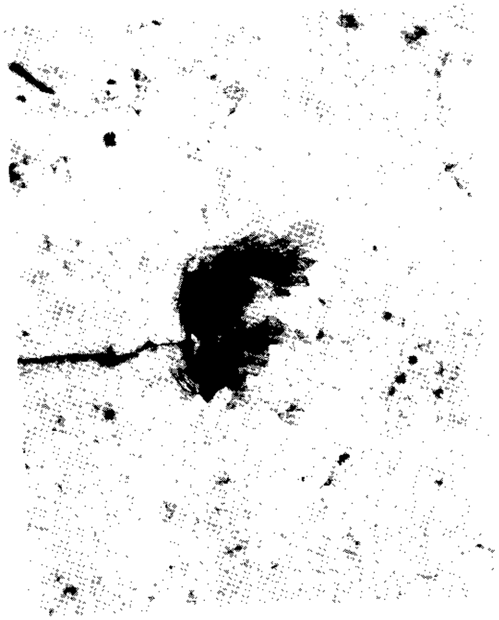

Fig. 14(c) Plate Surface.

Fig. 14(d) Plate Surface.

Fig. 14 PLASTIC ZONES DISPLAYED BY SAMPLE S-107 (Continued)

Fig. 14(e) Section 11.

Fig. 14(f) Section 22.

Fig. 14(g) Section 33.

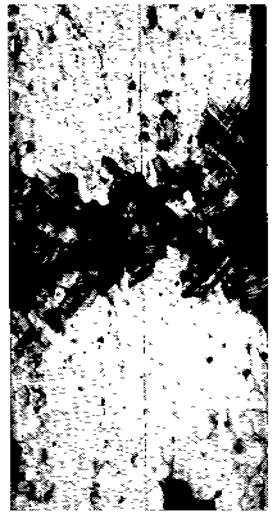

Fig. 14(h) Section 44.

Fig. 14(i) Section 55.

Fig. 14 PLASTIC ZONES DISPLAYED BY SAMPLE S-107 (Continued)

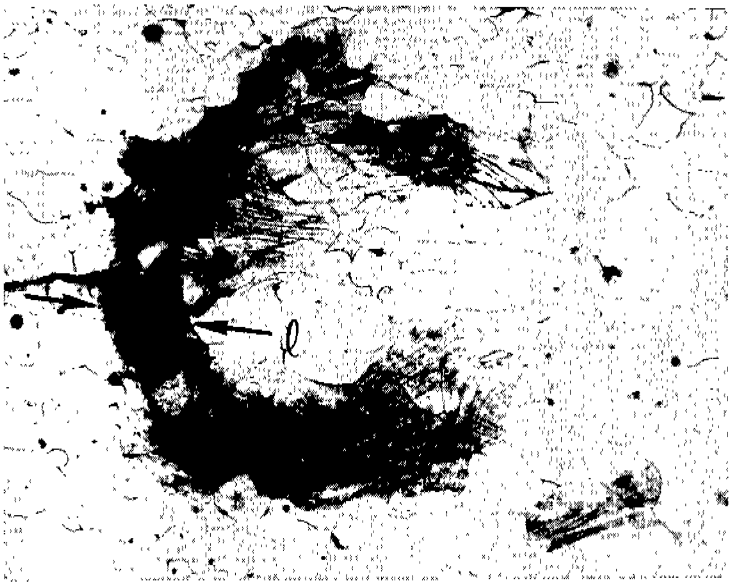

Fig. 15(a) Plate Surface.

Fig. 15(c) Plate Midsection.

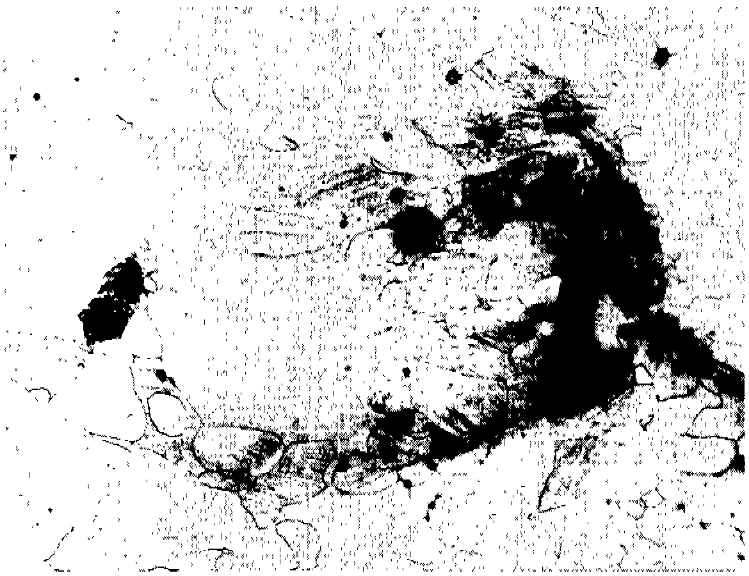

Fig. 15(b) Plate Surface.

Fig. 15 PLASTIC ZONES DISPLAYED BY SAMPLE GG-6 ($t = 0.220$ in, $\frac{K}{Y} = 0.33\ \sqrt{in}$): (a) and (b) are sections close to and parallel to the plate surface, (c) is the same crack as (a) observed on the midsection, (d) and (e) are interior sections of (b) close to the midsection and separated by about 0.020 in. 180X

Fig. 15(d) Plate Midsection.

Fig. 15(e) Plate Midsection.

Fig. 15 PLASTIC ZONES DISPLAYED BY SAMPLE GG-6 (Continued)

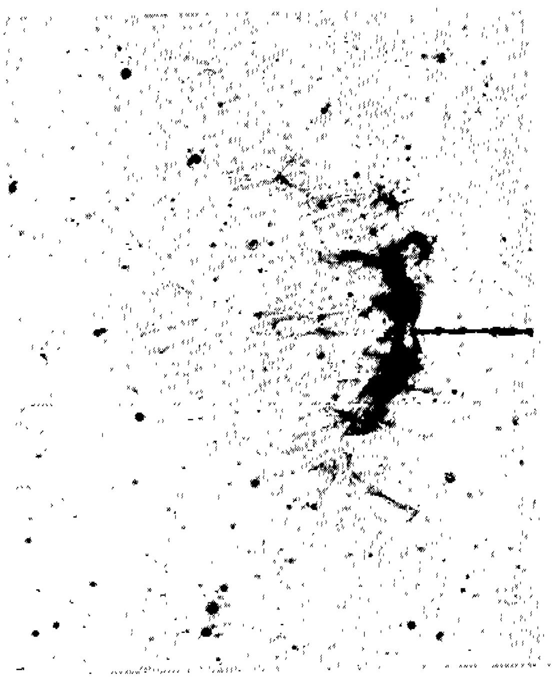

Fig. 16(a) Plate Surface.

Fig. 16(b) Plate Surface.

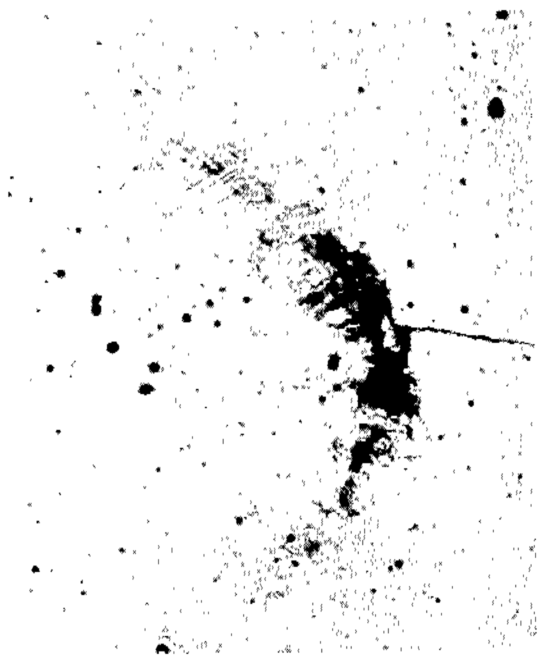

Fig. 16(c) Plate Midsection.

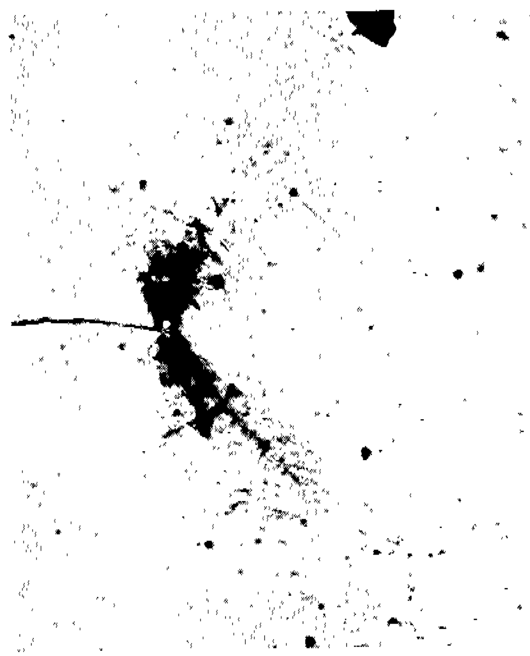

Fig. 16(d) Plate Midsection.

Fig. 16 PLASTIC ZONES DISPLAYED BY SAMPLE X-47 ($t = 0.420$ in, $\frac{K}{Y} = 0.38\ \sqrt{in}$): (a) and (b) on the plate surface, and (c) and (d) on the plate midsection. 45X

Fig. 17(a) X-47.

Fig. 17(b) X-47.

Fig. 17(c) X-49.

Fig. 17 PLASTIC ZONES DISPLAYED BY THE MIDSECTIONS OF SAMPLES: (a) and (b) X-47 (t = 0.420 in, $\frac{K}{Y}$ = 0.38 $\sqrt{in}$) and (c) X-49 (t = 0.420 in., $\frac{K}{Y}$ = 0.41 $\sqrt{in}$). 180X

Fig. 18(a) FF-3.

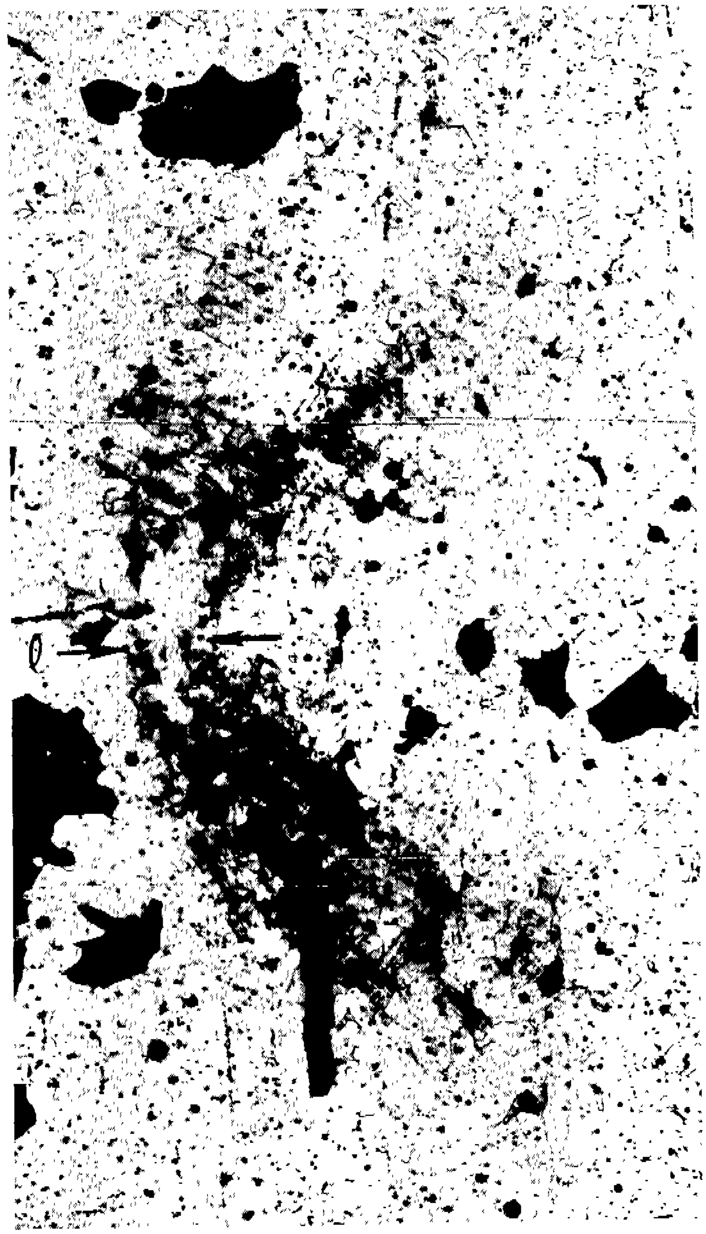

Fig. 18(b). FF-8.

Fig. 18 PLASTIC ZONES DISPLAYED BY THE MIDSECTIONS OF SAMPLES: (a) FF-3 ($t = 0.212$ in, $\frac{K}{Y} = 0.38\ \sqrt{in}$) and (b) FF-8 ($t = 0.212$ in, $\frac{K}{Y} = 0.46\ \sqrt{in}$). 45X

Fig. 19 PLASTIC ZONE DISPLAYED BY SAMPLE GG-5 (t = 0.220 in, $\frac{K}{Y}$ = 0.48 $\sqrt{in.}$) ON THE PLATE MIDSECTION PARALLEL TO THE SURFACE. 90X

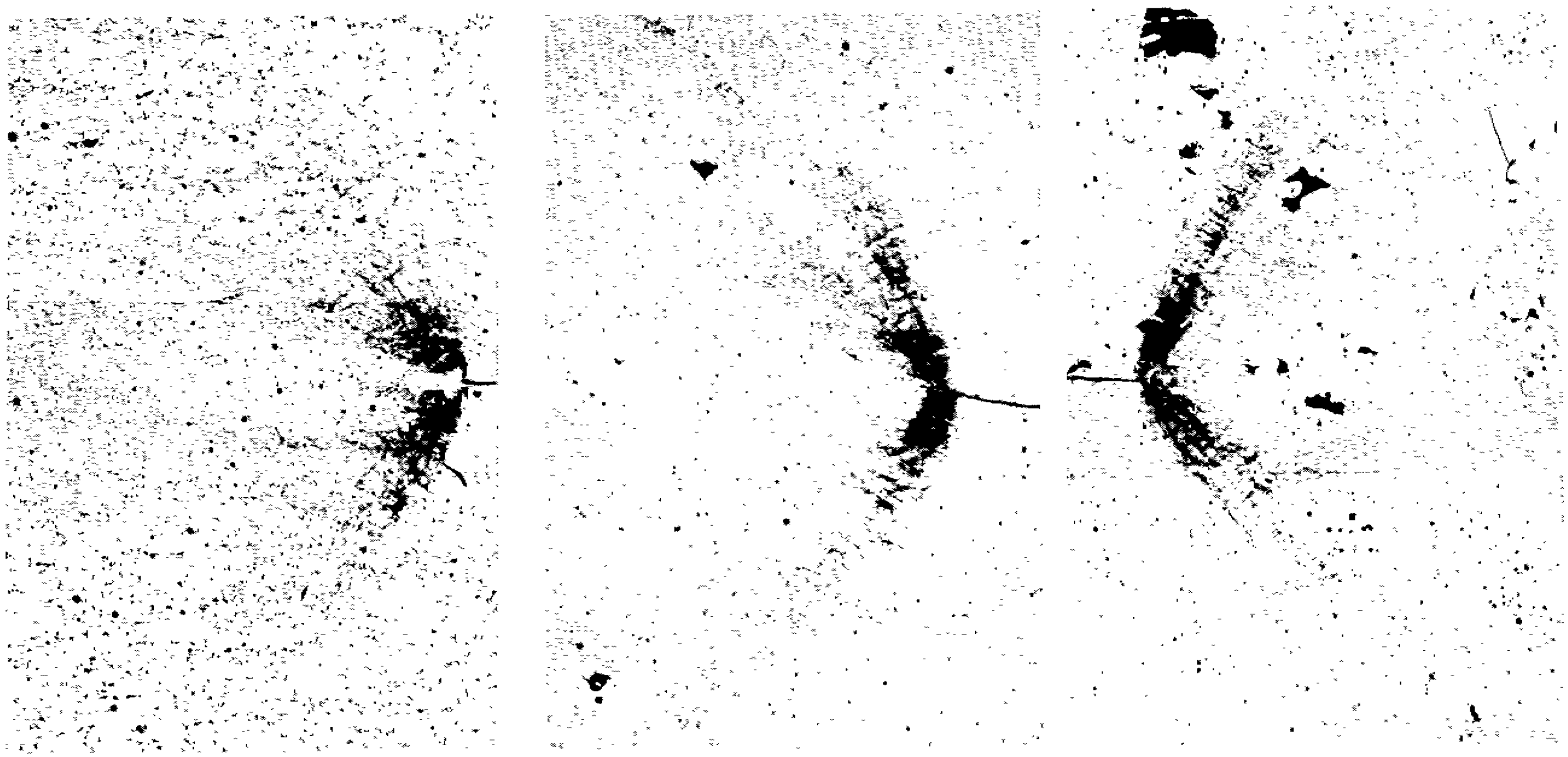

Fig. 20(a) Plate Surface. *Fig. 20(b) Plate Surface.* *Fig. 20(c) Plate Surface.*

Fig. 20 PLASTIC ZONES OBSERVED ON THE PLATE SURFACES OF SAMPLE X-46 ($t = 0.420$ in, $\frac{K}{Y} = 0.58\ \sqrt{in}$): (a) and (b) show the same crack tip viewed on opposite sides of the plate, and (c) is the other crack tip viewed on the same side as (b). 11X

Fig. 21(a) Plate Midsection.

Fig. 21(b) Plate Midsection.

Fig. 21. PLASTIC ZONES DISPLAYED BY SAMPLE X-46 ($t = 0.421$ in, $\frac{K}{Y} = 0.58\ \sqrt{in}$): (a) and (b) show the extremities of the center crack at 12X, and (c) shows the distribution of strain at the crack tip in (a) at 180X.

Fig. 21(c) Plate Midsection (Magnified Section of (a).

Fig. 21 PLASTIC ZONES DISPLAYED BY SAMPLE X-46 (Continued). Note that the grains identified as (1) are recovered rather than recrystallized, and not necessarily deformed.

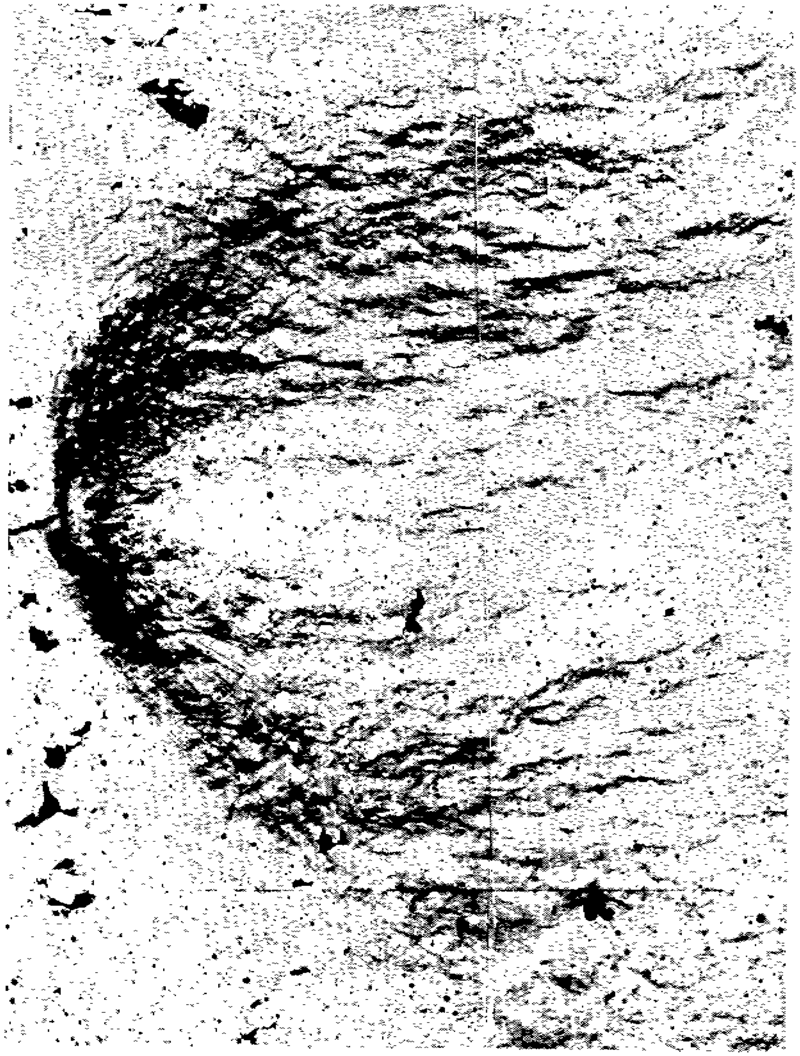

Fig. 22(a) Plate Surface.

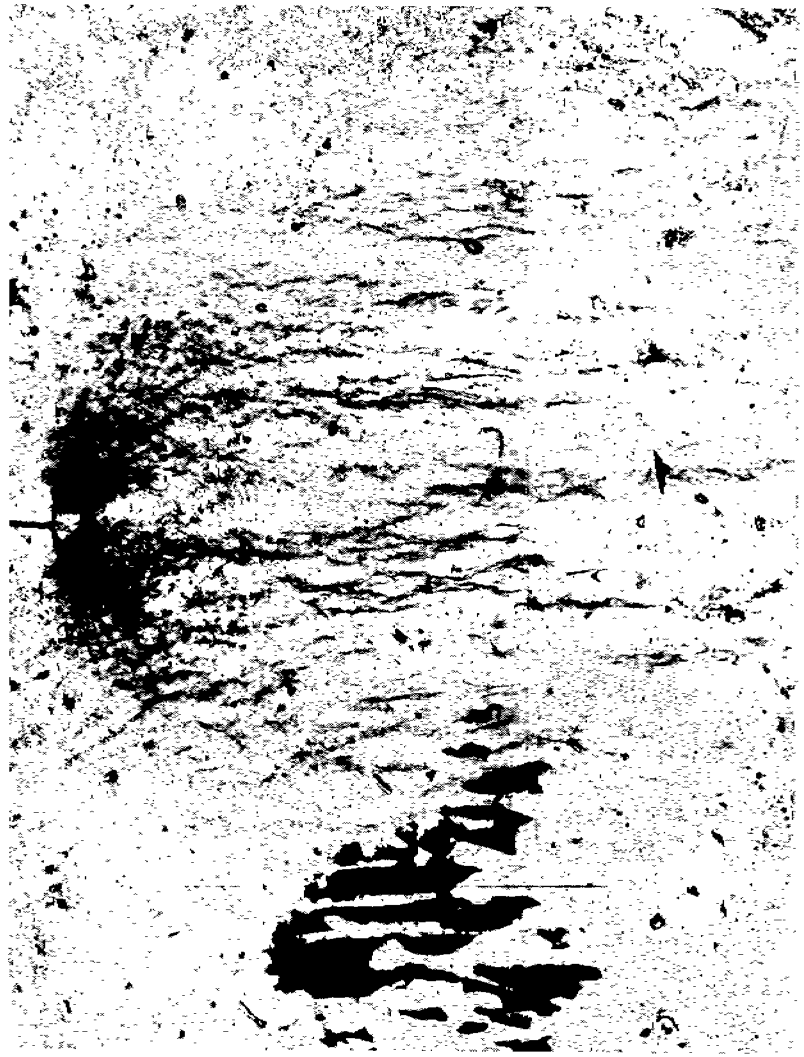

Fig. 22(b) Plate Midsection.

Fig. 22 PLASTIC ZONES DISPLAYED BY ONE OF THE EDGE CRACKS IN SAMPLE S-50 ($t = 0.420$ in, $\frac{K}{Y} = 0.73\ \sqrt{in}$): (a) plate surface, and (b) plate midsection. 11X

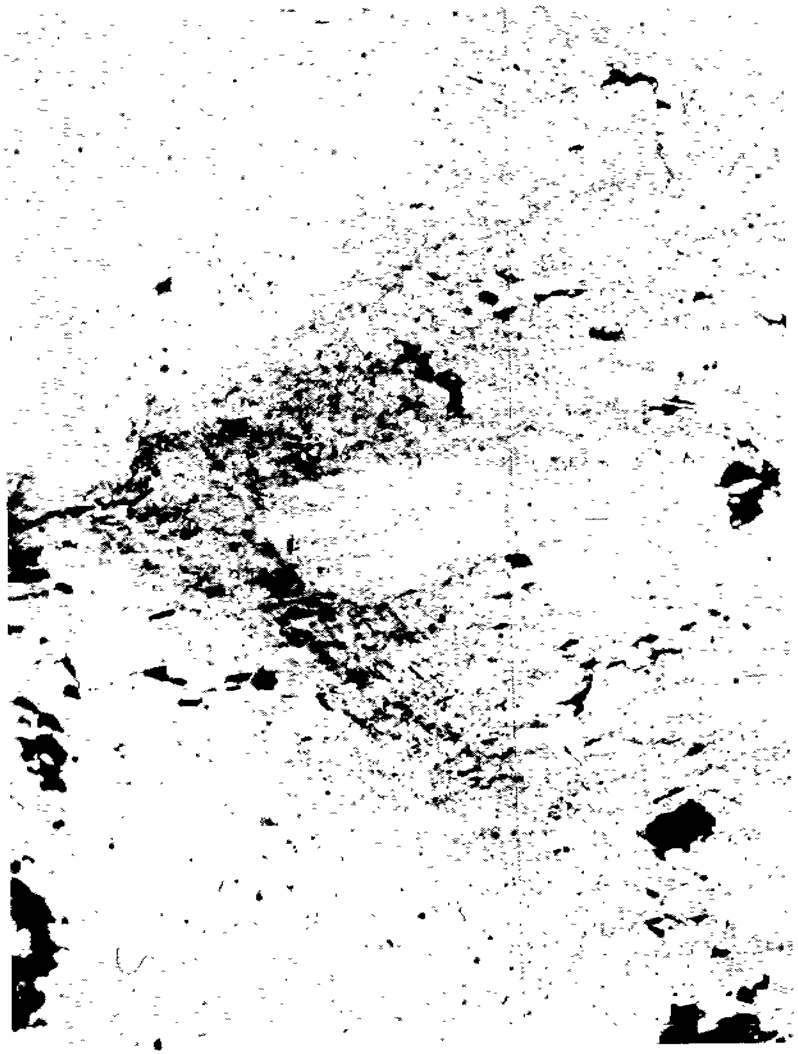

Fig. 23(a) Plate Surface.

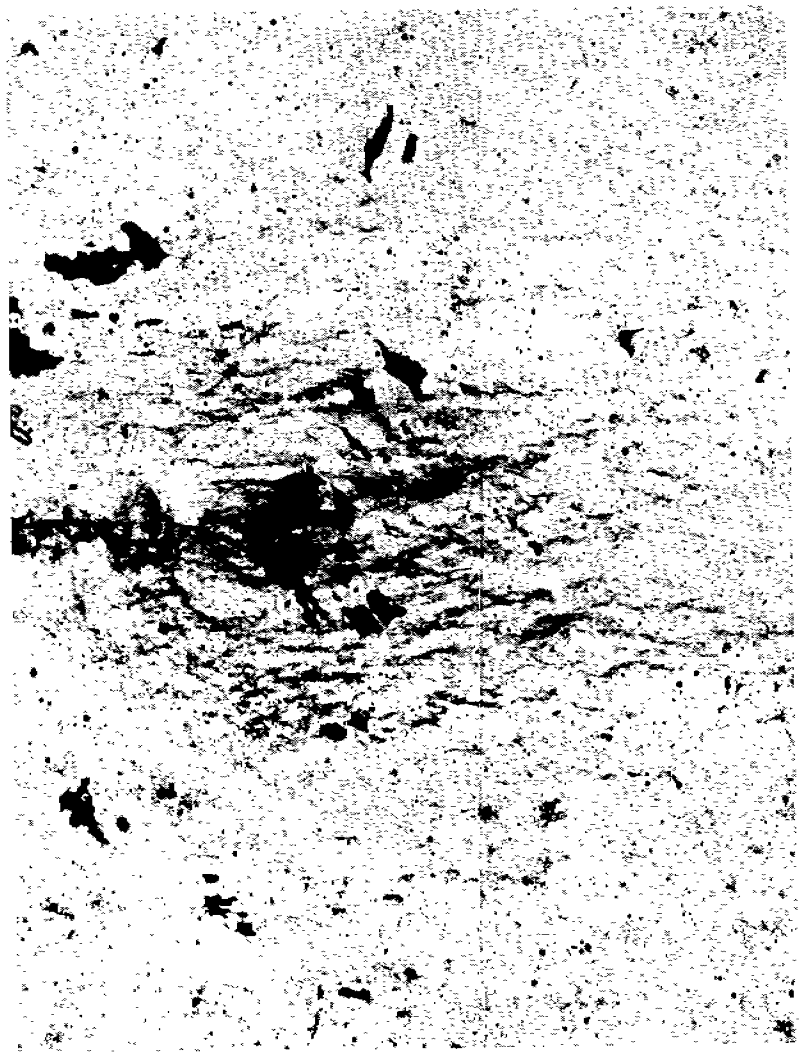

Fig. 23(b) Plate Midsection.

Fig. 23 PLASTIC ZONES DISPLAYED BY THE EDGE CRACK IN SAMPLE S-50 (t = 0.420 in, $\frac{K}{Y} = 0.73 \sqrt{in}$) OPPOSITE TO THE ONE SHOWN IN FIG. 22: (a) plate surface and (b) plate midsection. This crack underwent an increment of growth--about 0.05 in. on the midsection--giving the zone the unusual appearance. 11X

3. The fatigue precracks also presented a number of problems, especially in heats GG and FF. These cracks were not planar and their fronts tended to be oblique to the surface: some crack lengths varied by about 20% from one side of the plate to the other*. A few cracks were found to be segmented and not fully connected. For these reasons, the plastic zones generated by the fatigue cracks were not reproducible at stress levels below $K/Y = 0.2\sqrt{in.}$, and were more variable at the higher stress levels than the zones attending machined slits.

4. In one instance, reproduced in Figure 23, and 0.05 in.-increment of stable crack growth occurred in the course of the loading, and while the appearance of the added portion is indistinguishable from that of the original fatigue precrack, it is revealed by the etching, e.g., compare Figure 23 with Figure 22. In all other instances, the etched zones showed no evidence of stable growth.

5. Several other factors contributed to variability in the size and appearance of the zones including slight eccentricities in loading, local variations in grain size, grain orientation and etching response.

The large number of zones reproduced in this report are intended to establish features that are significant and reproducible. It is convenient to separate the plastic deformation into three components and these are shown schematically in Figure 24 (coordinates are identified in Figure 24(a)).

$\underline{\gamma_{xy,xy}\text{-Relaxation, Figures 24(a) and (b)}}$. In-plane deformation is produced by a system of shears, here identified by the symbol $\gamma_{xy,xy}$**, which is similar to the logarithmic spiral slip-line field (Figure 1(b)) combined with the elements of the punch slip-line field (Figure 1(a)). The spirals are not observed close to the plate surface***, but are seen on interior sections of the blunter machined slits; for example, Figures 6(b)-6(f) and 7(e) which display etched slip bands arranged in a pattern similar to the 'spiral' field. The spiral-like plastic zone that emerges from the slit first extends mainly in the x-direction to distances of the order of the root radius. Then the deformation reaches out in directions more nearly normal to the plane of the crack forming two wing-like, plastic zones each inclined at an angle $\theta \sim 65° \pm 8°$****

---

* The average length is quoted in Table 2.

** The notation $\gamma_{ij,k\ell}$ is intended to signify a strain field produced by shears on planes whose normals lie in the ij plane with the directions of shear also confined to the $k\ell$ plane.

*** Presumably because the z-direction stress is zero at the free surface.

**** Zones are curved and fan-shaped and do not present a well-defined inclination. θ should be regarded as the average inclination of the zone.

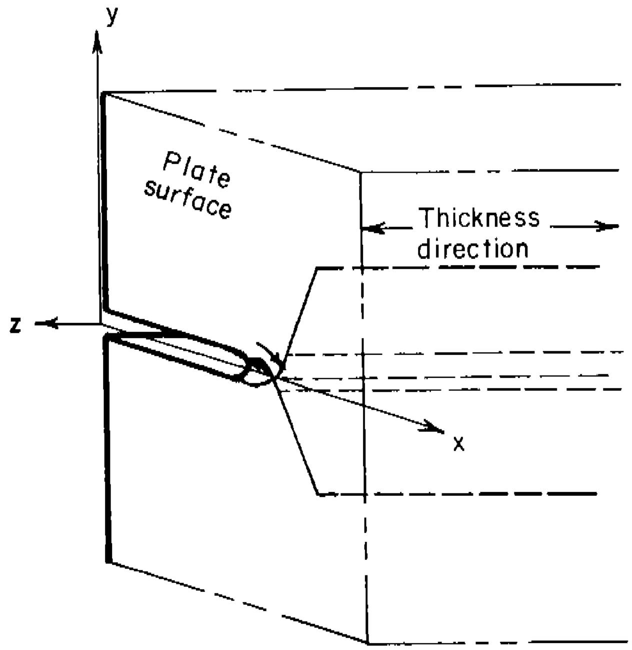

Fig. 24(a) $\gamma_{xy,\ xy}$ *(blunt notch).*

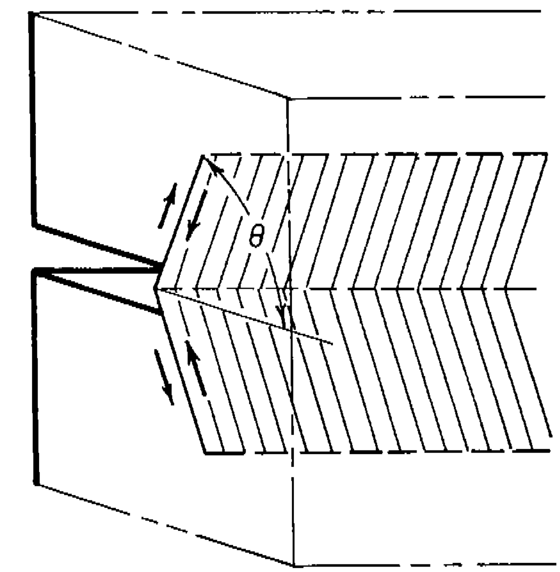

Fig. 24(b) $\gamma_{xy,\ xy}$ *(Sharp Crack).*

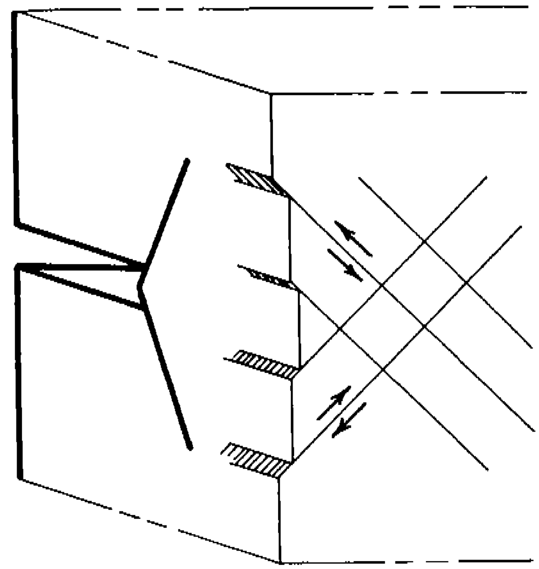

Fig. 24(c) $\gamma_{yz,\ yz}$.

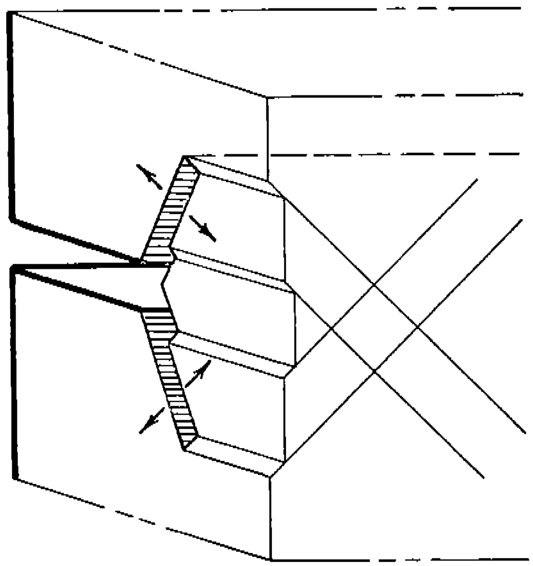

Fig. 24(d) $\gamma_{xy,\ yz}$.

Fig. 24 SCHEMATIC PICTURE OF THE THREE PLASTIC RELAXATION OBSERVED WITHIN THE PLASTIC ZONE: (a) and (b) show the in-plane shears labeled $\gamma_{xy,xy}$, *(c) and (d) show the through-the-thickness components,* $\gamma_{yz,yz}$ *and* $\gamma_{xy,yz}$.

(see Figure 24(b)). The character of slip within these zones is similar to the fan of the punch slip-line field (see, for example, Figures 7(e), 8(a), 9(e), 17, 18, 20, and 21). In Figure 7(e) slip lines having the "spiral" character extend in the x-direction to a distance of $\sim 2.5r$ (r is the root radius) from the notch root. According to slip-line field theory, σ_y, the normal stress acting at this distance, is 2.6 Y[(9)].****
In contrast, the spiral field of a sharp precrack is expected to be vanishingly small, giving rise to a slip-line field similar to the one for the V-notch charpy bar (see Figure 1(c) and Figure 24(b)). However, the highly strained portions of the zones of sharp cracks, which are revealed by the outline of the nonetching region in Figures 14(d), 17(a), 17(b), and 21(c), also show evidence of a spiral-like field close to the crack tip. This may be a consequence of the blunting of the crack tip or strain hardening.

$\gamma_{yz,yz}$-Relaxation, Figure 24(c). Figures 9, 10(b)-(e), and 14(e)-(i) are etched sections taken normal to the plate surface and these show deformation bands inclined at $\sim 45°$ to the y-direction. Since these bands are most prominent at the plate surface where $\sigma_y > \sigma_x < 0$ and $\sigma_z = 0$, they must represent $\gamma_{yz,yz}$, the component of plastic deformation in the thickness direction, rather than the in-plane strain $\gamma_{yz,xy}$. The $\gamma_{yz,yz}$-relaxation produces extensions in the tensile direction at the expense of measurable reductions in plate thickness. Like the plane stress solution described in Figure 1(e), which is related to it, the region of $\gamma_{yz,yz}$-relaxation extends in the x- and y-directions distances comparable to the extent of the $\gamma_{xy,xy}$ field. The etched sections in Figures 9 and 10 show that this deformation is more intense near the surface of the plate, but it extends roughly as far on interior sections as on the surface--a result that is a departure from the widely used picture of the "spool-shaped" zone proposed by Liu[(12)].

Perhaps the most unexpected result is shown in Figures 10(b)-(e), sections reflecting a stress level-thickness combination of $\left(\frac{K}{Y}\right)^2 \frac{1}{t} = 0.41$, which is widely regarded as a close approach to plane strain. In this case traces of plastic through-the-thickness relaxation still penetrate the entire plate. At higher applied stress levels, the $\gamma_{yz,yz}$-deformation in the Fe-3Si alloy tends to concentrate on two 45° inclined bands that intersect at the center of the plate and penetrate the entire section. The intersections of these bands with the plate surface are revealed by two horizontal wedge-shaped etching regions above and below the crack and one wedge in line with the crack on the plate midsection. Embryonic wedges of this type can be seen in Figures 11(a) and (c); and are described in more detail in References (19) and (20).

**** $\sigma_y = \frac{2Y}{\sqrt{3}} [1 + \ln (1 + x/r)]$, where x is the distance from the notch root, r is the root radius, and Y is the uniaxial yield stress.

It should be noted that the $\gamma_{yz,yz}$-relaxations are not always strongly etched on sections parallel to the plate surface (compare Figure 9(d) with 9(g). This may arise because the dislocations involved are largely in the plane of the plate and intersect parallel sections infrequently. It seems likely that etched sections parallel to the plate surface, such as Figures 16 and 20 which only contain evidence of in-plane deformation, are deceptive, especially since the surface displacement measurements in Table 3 show that through-the-thickness relaxation increases continuously with $\left(\frac{K}{Y}\right)^2 \frac{1}{t}$.

$\underline{\gamma_{xy,yz}\text{-Relaxation, Figure 24(d)}}$. The $\gamma_{yz,yz}$-field does not extend behind the crack front, but is accommodated near the front by shears similar to the ones identified here as $\gamma_{xy,yz}$-relaxation. This component does not stand by itself on any of the etched sections and is more difficult to identify. However, its presence is clearly revealed by the displacement contours derived from the interferometric patterns in Figure 12, which illustrate that the $\gamma_{xy,yz}$-zone is located just behind the crack front. The $\gamma_{xy,yz}$-deformation becomes apparent on etched sections when, surface and interior sections are compared. This is because the $\gamma_{xy,yz}$-deformation is symmetric about the center of the plate: vanishingly small on the midsection and most intense at the plate surface. For example, the dark etching region in Figure 11(a) that corresponds with displacements produced by $\gamma_{xy,yz}$-shears is absent in Figure 11(c).

The zone size can also be deduced from the etched sections, but comparisons with theory are not entirely straight forward. This is because "plane strain" calculations only consider $\gamma_{xy,xy}$-shears while the etched sections contain contributions from this and the $\gamma_{yz,yz}$ and $\gamma_{xy,yz}$ components. Two dimensions, ρ and ℓ, that come close to delineating the $\gamma_{xy,xy}$-zone, are identified in Figure 1, and measured values are quoted in Table 2 and Figures 25 and 26:

- ρ - The zone length is defined as the distance between the crack (or slit) root and the furthest extent of plasticity measured radially from the crack tip or the center of curvature of the slit

- ℓ - The width of the $\gamma_{xy,xy}$-zone at the slit or crack tip measured along the crack line.

The definition for ρ has the advantage that it is relatively unambiguous from an experimental standpoint. While it is not certain that the furthest extent of the zone corresponds to plane strain deformation, it seems likely that this is a reasonably good approximation as long as $\gamma_{xy,xy}$-deformation is the dominant component. For example, the results for samples S-57 and X-2 show that ρ-values are essentially independent of plate thickness in this range. On the other hand, the two ρ-values in Figure 25 for which through-the-thickness relaxation predominates, do fall on the high side. Zone lengths for the blunter slits appear to be systematically larger than for the sharp cracks, possibly because the slits were held under load for a longer period of time.

The measurement of ℓ is best accomplished on etched midsections since the $\gamma_{xy,yz}$-relaxation is absent here. The remaining $\gamma_{xy,xy}$-deformation can then be differentiated from $\gamma_{yz,yz}$ on the basis of the slip markings: the former produces etched slip markings with the spiral and fan character; the latter markings tend to

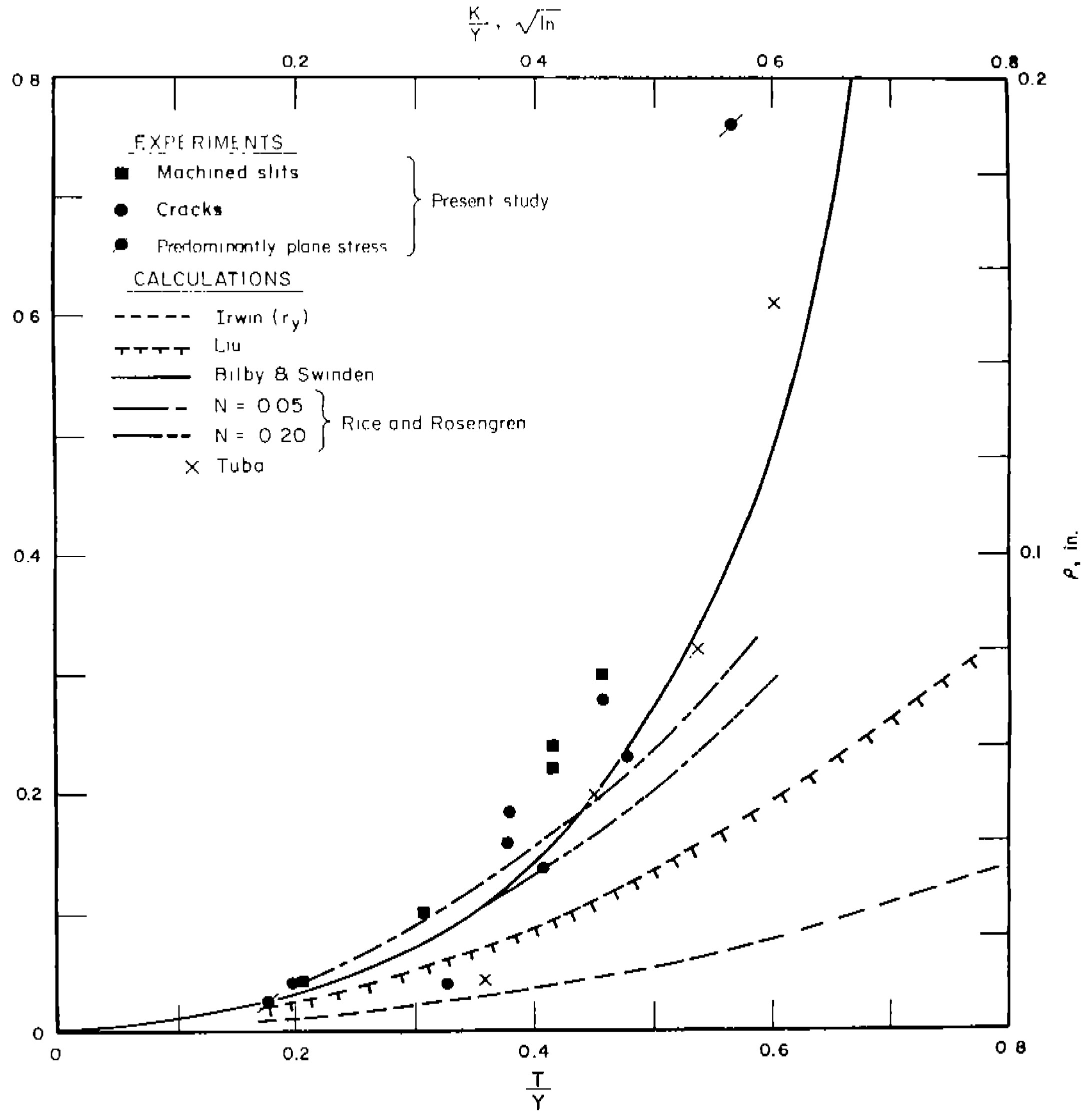

Fig. 25 COMPARISON OF MEASURED ZONE LENGTHS WITH VALUES DERIVED FROM VARIOUS THEORETICAL TREATMENTS 11-16. The $\frac{\rho}{a}$ scale (left) corresponds with the $\frac{T}{Y}$ scale (bottom); ρ (right) with $\frac{K}{Y}$ (top). The $\left|\frac{K}{Y}\right|$ scale is based on 0.25 in.-long edge cracks and the appropriate near-edge correction. All the theoretical curves were positioned with respect to the $\frac{K}{Y}$ scale.

be parallel to the x-axis (see Figure 24). The results of such measurements are plotted in Figure 26 in terms of the ratio $\frac{\ell}{\rho}$. This ratio does not appear to be a constant so that the zone width is not proportional to zone-length; the ratio $\frac{\ell}{\rho}$ decreases from about 0.35 to 0.05 as the stress level increases over the range examined. The width of the zones attending the slits appeared to be somewhat larger than for the cracks, a difference that is most probably related to the larger root radius of the slits.

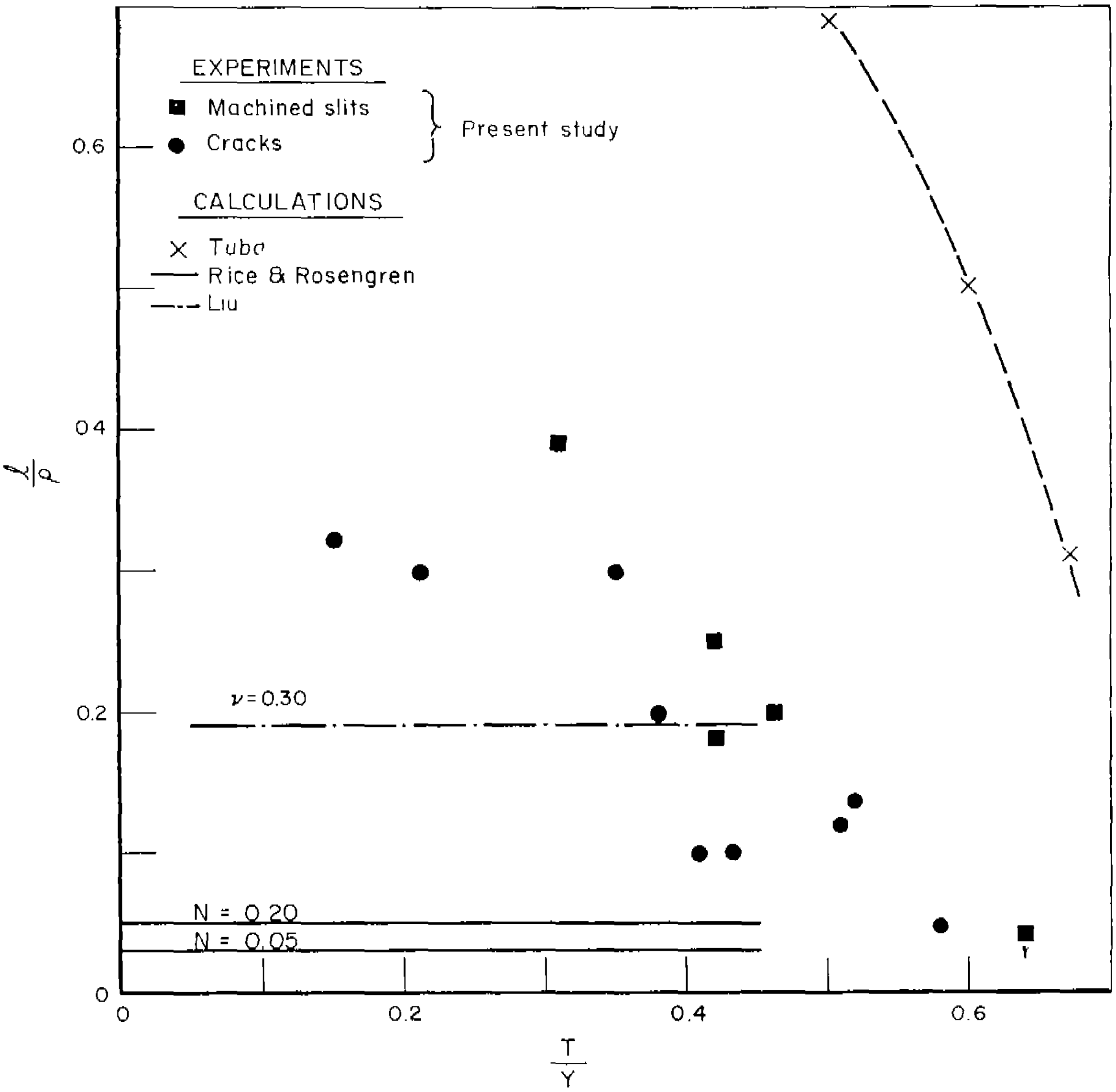

Fig. 26 COMPARISON OF MEASURED ZONE LENGTH-TO-WIDTH RATIOS WITH VALUES DERIVED FROM VARIOUS THEORETICAL TREATMENTS [12,14,15].

The through-the-thickness components are also important because of their influence on the triaxial stress state. Efforts were therefore made to characterize the contributions these make with the help of the following quantities which are described in Table 3 and Figure 27.

w - The maximum z-direction displacement of the plate surface produced by plastic deformation. Values were obtained by measuring the displacement of a point 0.001 in. and immediately ahead of the crack (or slit) tip relative to a point just outside the plastic zone, e.g., points (1) and (2) in Figure 12(b). These displacements were

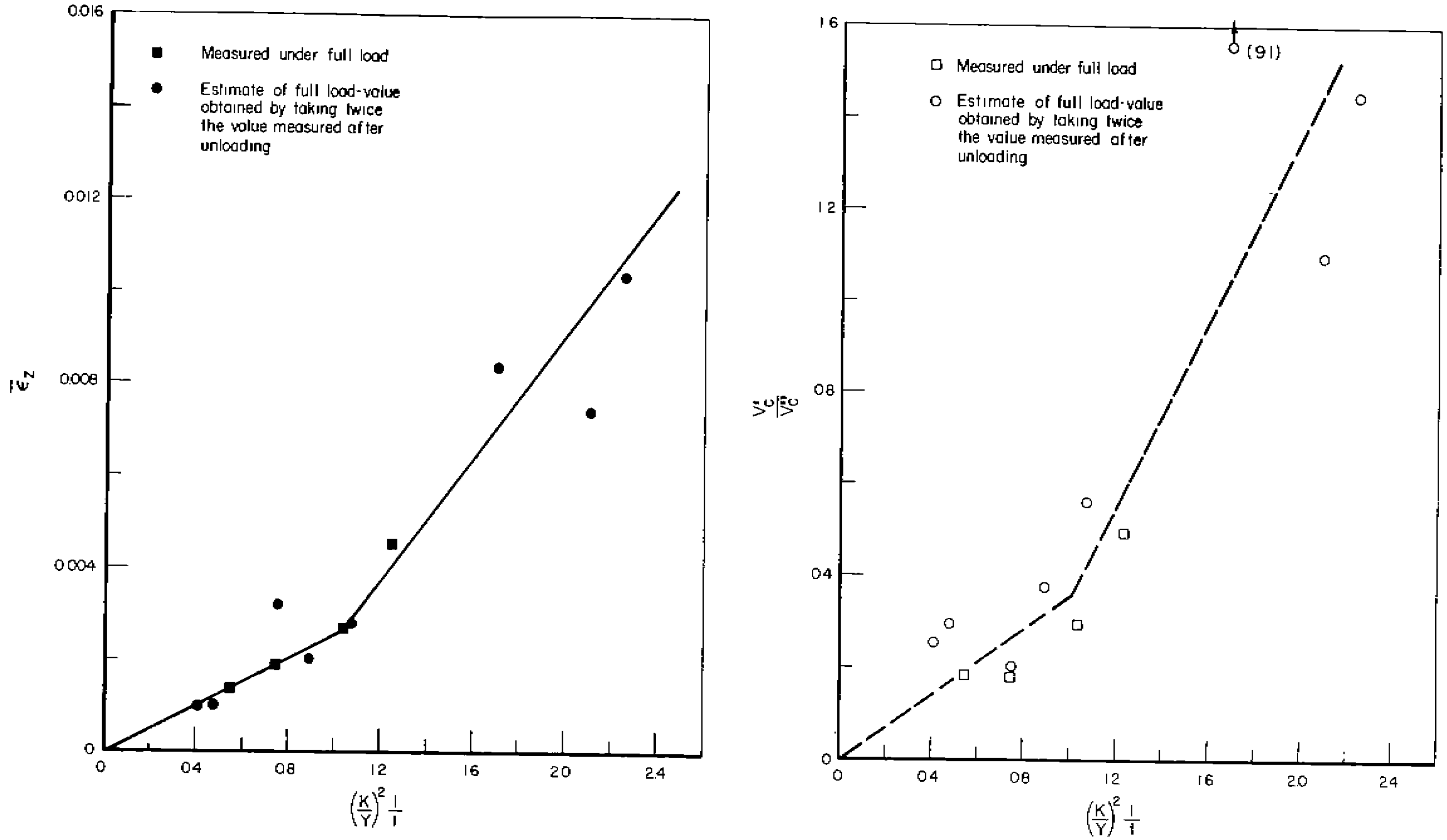

Fig. 27 INFLUENCE OF $\left|\frac{K}{Y}\right|^2 \frac{1}{t}$*, THE PLASTIC ZONE SIZE-PLATE THICKNESS PARAMETER, ON THROUGH-THE-THICKNESS DEFORMATION: (a) shows the influence on the average through-the-thickness strain* $\bar{\varepsilon}_z$*, (b) shows the effect on the plane stress-to-plane strain crack opening displacement ratio* $\frac{v'_c}{v''_c}$.

obtained under full load from the plastic replicas of the surface, and after unloading from the interferometric fringe patterns. Iso-displacement contours obtained from such patterns are reproduced in Figure 12.

$\bar{\epsilon}_z$ - The average strain at the crack tip corresponding to w: $\bar{\epsilon}_z = \frac{2w}{t}$ (where t is the plate thickness).

v'_c - The crack opening displacement at the crack tip produced by through-the-thickness deformation. An estimate of the average displacement over the plate cross section is obtained from the surface displacement measurements*:

$$v'_c \approx -\frac{1}{t}\int_{y=0}^{y=\infty} w\, dy \qquad (1)$$

v''_c - The crack opening displacement produced by in-plane relaxation. Estimates of this value were obtained from Bilby and Swinden's theoretical expression**:

$$v''_c = \frac{2Ya}{\pi E}\, \ln\, \sec\frac{\pi T}{2Y} \qquad (2)$$

A comparison of the w-values obtained for samples X-2 and X-3 (the two samples possess the same thickness and were loaded to about the same stress level, see Table 3) indicates that values measured under load are approximately twice the value measured after unloading. The factor 2 is consistent with theoretical expectations[6,31] and was used to convert residual displacement measurements into estimates of the full-load values. Figure 27(a) presents more evidence favoring this approximation. $\bar{\epsilon}_z$-values derived from full-load w-measurements are in good accord with the estimate obtained by taking 2x the w-value measured after unloading. The results in Figure 27(a) also illustrate that $\bar{\epsilon}_z$ increases continuously with $\left(\frac{K}{Y}\right)^2 \frac{1}{t}$ over the range examined and that small but measurable through-the-thickness strains are observed under conditions normally regarded as plane strain, i.e., $\left(\frac{K}{Y}\right)^2 \frac{1}{t} < 0.4$.

The ratio $\frac{v'_c}{v''_c}$ is more meaningful in this respect, because it expresses the relative contributions of through-the-thickness and in-plane deformation to the blunting of the crack. The plot in Figure 27(b) thus indicates that through-the-thickness relaxation already makes a significant contribution at $\left(\frac{K}{Y}\right)^2 \frac{1}{t} = 0.4$ and becomes the dominant mode $\frac{v'_c}{v''_c} \geq 1$ when $\left(\frac{K}{Y}\right)^2 \frac{1}{t} = 1.7$, or equivalently when $\rho \approx \frac{t}{2}$. This last result is consistent with expectations for $\gamma_{yz,yz}$-deformation*** (20) and

---

* Assuming plastic deformation proceeds without a volume change, and that strains are zero in the x-direction.

** Since the Bilby-Swinden model provides a relatively good description of ρ (see Figure 25), it was assumed that it would also provide a reasonable estimate of v''_c. In Equation (2), E is Young's modulus.

*** Since $\gamma_{yz,yz}$-slip bands are inclined ~45° to the tensile axis, they are not impeded by elastic regions and can freely penetrate the entire plate when $\rho \approx \frac{t}{2}$.[20]

this provides some support for the method of formulating the $\frac{v_c'}{v_c''}$ -ratio. The interpretation of $\frac{v_c'}{v_c''}$ -values is complicated by the fact that through-the-thickness relaxation is more intense near the plate surface than in the interior under conditions approaching plane strain. As a result, values of the $\frac{v_c'}{v_c''}$ -ratio appropriate for the plate midsection are smaller than the average values quoted in Figure 27(b) in the range $0 < \left(\frac{K}{Y}\right)^2 \frac{1}{t} < 1$. This also means that the change from predominantly plane strain to predominantly plane stress in the vicinity of $\left(\frac{K}{Y}\right)^2 \frac{1}{t} \approx 1$ is probably marked by $\frac{v_c'}{v_c''}$ -transition that is more abrupt than the one revealed in Figure 27(b). The various displacement values quoted, together with the dimensions of the plastic zone also provide a way of estimating average strains and this is illustrated in Table 4.

IV. DISCUSSION

Comparisons with the theoretical treatments of plane strain deformation identified in Figure 1 show that Tuba's[14] enclaves reproduce the general shape of the experimental $\gamma_{xy,xy}$-field to a good approximation. For example, the 68° inclination suggested by Tuba's zones agrees with the 65° ± 8° value derived from the etchings. The measured ρ-values are also in good accord with Tuba's measurements*, and they are also closely represented by the Bilby-Swinden[13] expression (quoted in Figure 1(c)) and the Rice and Rosengren[15] result (Figure 1(b)). However, the Rice and Rosengren zones display a backward tilt not observed in practice. According to Rice[32], this tilt may be a consequence of assigning a Poisson's ratio of 1/2 to the elastic as well as the plastic region, an oversimplification Rice is now attempting to correct. Calculations based on the elastic stress field such as Liu's[12] treatment, tend to underestimate ρ.

Irwin's generalized zone parameter, r_y, also grossly underestimates ρ; r_y does provide reasonable estimates of ℓ (the one parameter with which it really should be compared) in the K/Y range examined here, but its stress dependence is the same as ρ, which is not confirmed by the experiments. Rice and Rosengren grossly underestimate ℓ at low stress levels. The proportions of Liu's zone are more realistic than those derived from the Rice and Rosengren treatment, but neither predict a variation in the $\frac{\ell}{\rho}$ ratio. Tuba's treatment does reproduce the change in $\frac{\ell}{\rho}$ but overestimates the values of this ratio. It appears that none of the current theoretical treatments provides a satisfying description of the zone width-ℓ, which suggests that these treatments may also encounter difficulties in describing the strain distribution within the zone. For example, the results for sample S-107 illustrate that the peak strain is already in excess of 0.03** at a stress intensity level $\frac{K}{Y} = 0.21$ in. ($\frac{T}{Y} = 0.21$). So far, only Tuba has calculated strain profiles and he shows a peak plastic strain of about 0.002 at the crack tip at a stress level of $\frac{T}{Y} = 0.67$. However, the two results are not comparable since the strain in advance of the crack is governed by $\frac{K}{Y}$ rather than $\frac{T}{Y}$ (Tuba's crack length is not stated in absolute terms). Furthermore, the strains calculated by Tuba near the crack tip may still be influenced by the mesh size[14].

---

* The value quoted for $\frac{T}{Y} = 0.4$ possibly suffers inordinantly from an inadequate mesh size.

** The light etching region shows that the strain is in excess of 0.05 after unloading. Approximately 1/3 of this occurred while the load was removed; the full-load value was thus approximately 2/3 of 0.005 or 0.003.

TABLE 4. ESTIMATES OF IN-PLANE AND THROUGH-THE-THICKNESS PLASTIC STRAINS IN THE VICINITY OF THE CRACK TIP

		In-Plane Deformation					Through-The-Thickness Deformation			
Sample No.	$\frac{K}{Y}$ ($\sqrt{\text{in.}}$)	(a) ℓ (in.)	(b) $2v''_c$ (10^{-5} in.)	(c) $\bar{\gamma}_{xy,xy}$	(d) $\bar{\epsilon}_{xy,xy}$	(e) $\epsilon_{xy,xy}$ (max)	(f) ℓ' (in.)	(g) $v_{xy,yz}$ (10^{-5} in.)	(h) $\bar{\gamma}_{xy,yz}$	(i) $\bar{\epsilon}_{xy,yz}$
S-107 (crack)	0.21	0.003	4.8	0.016	0.008	> 0.03	-	-	-	-
S-57 (slit)	0.42	0.010	20	0.020	0.010	> 0.03	0.006	16	0.027	0.014
S-60 (slit)	0.64	0.020	54	0.027	0.014	> 0.03	0.024	60	0.025	0.013

(a) Zone width, as previously defined.

(b) v''_c is the component of crack opening displacement at the crack (or slit) tip produced by in-plane ($\gamma_{xy,xy}$) relaxations. Values quoted are estimates based on the Bilby-Swinden[13] model: $v''_c = \frac{2Ya}{\pi E} \ln \sec \frac{\pi T}{2Y}$

(c) $\bar{\gamma}_{xy,xy} \equiv \frac{2v''_c}{\ell}$ is the average in-plane plastic shear strain in zone just ahead of crack.

(d) $\bar{\epsilon}_{xy,xy}$ is the tensile strain corresponding to $\bar{\gamma}_{xy,xy}$: $\bar{\epsilon}_{xy,xy} = \frac{1}{2}\bar{\gamma}_{xy,xy}$.

(e) Peak tensile strain at the crack tip deduced from etching response.

(f) ℓ' is the width of $\gamma_{xy,yz}$-zone near crack tip as denoted by arrows in Figure 12.

(g) $v_{xy,yz}$ is the full load (or 2x the residual) z-direction displacement over the distance ℓ' marked by arrows in Figure 12.

(h) $\bar{\gamma}_{xy,yz} \equiv \frac{v_{xy,yz}}{\ell'}$ is the average $\gamma_{xy,yz}$-shear strain at the crack tip and plate surface.

(i) $\bar{\epsilon}_{xy,yz}$ is the average tensile strain corresponding to $\bar{\gamma}_{xy,yz}$: $\bar{\epsilon}_{xy,yz} = \frac{1}{2}\bar{\gamma}_{xy,yz}$.

The results may also be compared with plastic zones produced by Clark[24] in 1-in. thick, compact tension (double cantilever beam) specimens of Fe-3Si (heat GG) and revealed by the etching technique described here. While their appearance is quite similar, Clark's zones are only about half as large at comparable stress intensity levels as the zones described here. Recent calculations by Wilson[33] indicate that this difference is a consequence of the finite dimensions of the compact tensile specimen and their influence on the stress field.

Values of the ratio $\frac{v'_c}{v''_c} < 1$ are evidence that the in-plane ($\gamma_{xy,xy}$) component is the dominant relaxation. While this dominance and the approach to plane strain are synonymous, the plane strain state is only attained in the limit $\frac{v'_c}{v''_c} \rightarrow 0$. Conversely, increasing values of $\frac{v'_c}{v''_c}$ signify a shift away from plane strain in the general direction of plane stress. Figure 27(b) shows that the $\frac{v'_c}{v''_c}$ ratio begins to increase more rapidly beyond $\left(\frac{K}{Y}\right)^2 \frac{1}{t} > 1$ or, equivalently, beyond $\rho = \frac{t}{4}$. The change could be a sign of the beginning of a rapid loss of constraint and triaxiality and, thus, could provide a basis for fixing a practical upper bound to the plane strain region. For example, the authors have shown in a related paper[3] that fracture toughness values become sensitive to the thickness at a stress intensity level-thickness combination closer to $\left(\frac{K}{Y}\right)^2 \frac{1}{t} = 1$ than to 0.4. More displacement measurements of this type on other materials would be desirable to affirm this conclusion. By the same token, the dominance of through-the-thickness deformation and the approach to plane stress are synonymous. However, this does not mean that z-direction stresses within the zone are completely relaxed when $\frac{v'_c}{v''_c} \geq 1$. It seems likely that the plane stress state is only attained in the limit $\left(\frac{v'_c}{v''_c}\right) \rightarrow \infty$. It is possible that displacement measurements could also be of value in setting a practical lower bound to the plane stress region.

V. CONCLUSIONS

1. Three types of plastic relaxation are observed within the plastic zones produced by both sharp cracks and by blunt notches; one component is confined to the plane of the plate (plane strain) and two accommodate through-the-thickness deformation. Under conditions approaching plane strain in-plane deformation is the predominant mode, but traces of plastic through-the-thickness deformation still penetrate the entire plate at $\left(\frac{K}{Y}\right)^2 \frac{1}{t} = 0.41$.

2. Theoretical treatments of the plane strain zone by Bilby and Swinden, by Tuba and by Rice and Rosengren are in good accord with measurements of the maximum extent of the zone. The zone width (measured at the crack tip) does not appear to be proportional to the zone length; the width to length ratio decreases from 0.35 to 0.05 as the stress intensity level is increased in the range from $\frac{K}{Y} = 0.2\sqrt{\text{in.}}$ to $0.6\sqrt{\text{in.}}$ None of the existing theoretical treatments offer a really satisfactory description of this dimension.

3. The etching reveals that the in-plane deformation within the plastic zone is produced by a system of shears similar to the logarithmic spiral slip-line field combined with elements of the punch field. This part of the zone is best revealed on the plate midsection. The etching also provides insights to character and location of shears responsible for through-the-thickness deformation and the magnitude of the plastic strains generated within the zone. For example, the peak strain at the tip of a sharp crack already exceeds 0.03 when $\frac{K}{Y} = 0.21\sqrt{\text{in.}}$

4. Surface displacement measurements indicate there is an increase in the rate at which through-the-thickness deformation accumulates relative to in-plane deformation when $\left(\frac{K}{Y}\right)^2 \frac{1}{t} > 1$. This change may serve to identify a practical upper bound to the plane strain regime. The displacement measurements also suggest that through-the-thickness deformation is the dominant mode of relaxation when $\left(\frac{K}{Y}\right)^2 \frac{1}{t} > 1.7$, but this is not necessarily equivalent to a close approach to a state of plane stress.

VI. ACKNOWLEDGMENTS

The authors are grateful to the Ship Structure Committee, who supported this project. They wish to thank A. R. Lytle, R. W. Rumke, and the members of the Ship Hull Research Committee whose guidance contributed in an important way to the success of the project. They also wish to acknowledge the essential contributions of P. Mincer and R. Stephenson who performed the bulk of the experimental work, especially the painstaking metallographic studies. The authors also wish to thank M. F. Kanninen and S. Kobayashi for fruitful discussions, and C. Pepper for her work on the manuscript.

VII. REFERENCES

1. F. A. McClintock and G. R. Irwin, "Plasticity Aspects of Fracture Mechanics", Am. Soc. Test Mat'ls. STP 381, p. 84, 1965.

2. J. M. Krafft, "Correlation of Plane Strain Crack Toughness with Strain Hardening Characteristics of a Low, a Medium, and a High Strength Steel", App. Matls. Res., Vol. 3, p. 88, 1963.

3. G. T. Hahn and A. R. Rosenfield, "Sources of Fracture Toughness: The Relation Between K_{Ic} and the Ordinary Tensile Properties of Metals", Am. Soc. Test. Mat'ls. STP 432, p. 5, 1968.

4. D. N. de G. Allen and R. Southwell, "Plastic Straining in Two Dimensional Stress-Systems", Phil. Trans., Roy. Soc. of London, Ser. A, Vol. 242, p. 379, 1949-1950.

5. J. A. Jacobs, "Relaxation Methods Applied to the Problem of Plastic Flow, Notched Bar under Tension", Phil. Mag., Ser. F, Vol. 41, p. 349, 1950.

6. J. A. Hult and F. C. McClintock, "Elastic-Plastic Stress and Strain Distribution Around Sharp Notches Under Repeated Shear", IXth International Congress Applied Mechanics, 8, p. 51, Brussels, 1956.

7. F. A. McClintock, Discussion to, "Fracture Testing of High Strength Sheet Materials", Mat'ls. Res. and Stands., Vol. 1, p. 277, 1961.

8. L. Prandtl, Nachr. Ges. Wiss. Göttingen, p. 74, 1920.

9. R. Hill, "The Mathematical Theory of Plasticity", p. 245, Oxford, London, 1950.

10. A. P. Green, Quarterly J. Mech. Appl. Maths., Vol. 6, p. 223, 1953.

11. G. R. Irwin, "Dimensional and Geometric Aspects of Fracture", Fracture of Engineering Materials, p. 211, ASM, Ohio, 1964.

12. H. W. Liu, Discussion to: "The Effect of Size and Stress History on Fatigue Crack Initiation and Propagation", Proc. Cranfield Crack Prop. Symp., Vol. 2, p. 514, 1962.

13. B. A. Bilby and K. H. Swinden, "Representation of Plasticity at Notches by Linear Dislocation Arrays", Proc. Roy. Soc., Ser. A, Vol. 285, p. 22, 1965.

14. I. S. Tuba, A Method of "Elastic-Plastic Plane Stress and Strain Analysis", J. Strain Analysis, Vol. 1, p. 115, 1966.

15. J. R. Rice and G. F. Rosengren, "Plane Strain Deformation Near A Crack Tip in a Power-Law Hardening Material", J. Mech. Phys. Solids, Vol. 16, p. 1, 1968.

16. G. R. Irwin, J. M. Krafft, P. C. Paris, and A. A. Wells, "Basic Aspects of Crack Growth and Fracture", NRL Report 6598, Nov. 1967.

17. A. P. Green and B. B. Hundy, "Initial Plastic Yielding in Notch Bend Tests", J. Mech. Phys. Solids, Vol. 4, p. 128, 1956.

18. J. R. Low, Jr. and R. W. Guard, "The Dislocation Structure of Slip Bands in Iron", Acta Met., Vol. 7, p. 171, 1959.

19. Ship Structure Committee Report-165, Dec. 1964, G. T. Hahn and A. R. Rosenfield, "Local Yielding and Extension of a Crack Under Plane Stress, Acta Met., Vol. 13, p. 293, 1965.

20. Ship Structure Committee Report-172, March 1966, P. K. Dai and G. T. Hahn, "Crack Extension and Propagation Under Plane Stress", Proc. First Int. Conf. Fracture, Vol. 1, p. 223, 1965.

21. Ship Structure Committee Report-179, Nov. 1966, J. Cammett, A. R. Rosenfield, and G. T. Hahn, "Residual Strains and Displacements Within the Plastic Zone Ahead of a Crack".

22. Ship Structure Committee Report-180, Dec. 1966, G. T. Hahn and A. R. Rosenfield, "Experimental Determination of Plastic Constraint Ahead of a Sharp Crack Under Plane-Strain Conditions", Trans ASM, Vol. 59, p. 909, 1966.

23. G. T. Hahn and A. R. Rosenfield, "Plastic Zones Generated by Cracks Growing Under Load", Int. J. Fracture Mech. (to be published).

24. W. G. Clark, Jr., "Visual Observation of the Crack Tip Plastic Zone Developed in a 3 Per Cent Si-Fe Alloy", Westinghouse Scientific Paper, 66-1D6-BTLFR-P1, September 27, 1966.

25. Proposed Recommended Practice For Plane-Strain Fracture Toughness Testing of High Strength Metallic Materials Using a Fatigue-Cracked Bend Specimen, to be published in the 1968 Am. Soc. Test. Matls. Standards, Part 31 (green pages-for information only).

26. P. C. Paris and G. C. Sih, "Stress Analysis of Cracks", Am. Soc. Test. Matls. STP 381, p. 30, 1965.

27. A. K. Mukherjee, A. R. Rosenfield, L. E. Hulbert, and G. T. Hahn, "Notch Behavior in Metals", Air Force Matls. Lab. Report AFML-TR-66-266, 1966.

28. G. U. Oppel and P. W. Hill, "Strain Measurements at the Root of Cracks and Notches", Exp. Mech., Vol. 4, p. 206, 1964.

29. C. E. Morris, "Electropolishing of Steel in Chrome Acetic Acid Electrolyte", Metal Progress, Vol. 56, p. 696, 1949.

30. J. C. Suits and J. R. Low, Jr., "Dislocation Etch Pits in Silicon Iron", Acta Met., Vol. 5, p. 285, 1957.

31. J. R. Rice, "Plastic Yielding at a Crack Tip", Proc. First Int. Conf. on Fracture, Vol. 1, p. 283, 1965.

32. J. R. Rice (private communication).

33. W. K. Wilson, "Geometry and Loading Effects on Elastic Stresses at Crack Tips", Westinghouse Research Report 67-1D7-BTLPV-R1, July 3, 1967.

NONE

Security Classification

DOCUMENT CONTROL DATA - R&D		
(Security classification of title, body of abstract and indexing annotation must be entered when the overall report is classified)		
1. ORIGINATING ACTIVITY (Corporate author) Battelle Memorial Institute	2a. REPORT SECURITY CLASSIFICATION UNCLASSIFIED 2b GROUP	
3 REPORT TITLE Plastic Flow In The Locale On Notches And Cracks In Fe-3Si Steel Under Conditions Approaching Plane Strain.		
4. DESCRIPTIVE NOTES (Type of report and inclusive dates)		
5. AUTHOR(S) (Last name, first name, initial) G. T. Hahn and A. R. Rosenfield		
6. REPORT DATE November 1968	7a. TOTAL NO. OF PAGES 53	7b. NO. OF REFS 33
8a. CONTRACT OR GRANT NO. Nobs - 92383 b. PROJECT NO. SR-164 c. d.	9a. ORIGINATOR'S REPORT NUMBER(S) 9b. OTHER REPORT NO(S) (Any other numbers that may be assigned this report) SSC-191	
10 AVAILABILITY/LIMITATION NOTICES Distribution of this document is unlimited.		
11. SUPPLEMENTARY NOTES	12. SPONSORING MILITARY ACTIVITY	

13 ABSTRACT

The development of the plastic zones generated by sharp through-cracks and blunter notches was studied systematically in plates of Fe-3Si steel. A sensitive etching technique revealed the plastic zone both on the plate surface and on parallel and normal interior sections. In addition, the progress of through-the-thickness deformation was followed by monitoring normal displacements at the plate surface. The work encompasses applied stress-crack length-thickness combinations in the range $0.2 < \left|\frac{K}{Y}\right|^2 \frac{1}{t} < 2$ (K is the stress intensity parameter, Y is the yield stress, and t is the plate thickness), with special emphasis on situations where the plastic zone is small relative to the plate thickness and a plane strain state is approached. Three kinds of relaxations are revealed: one in the plane of the plate and two accomodating through-the-thickness deformation. The latter become the dominant mode when $\left|\frac{K}{Y}\right|^2 \frac{1}{t} > 1.7$ or $\rho \gtrsim \frac{t}{2}$ (ρ is the zone length). Comparisons with available theoretical treatments show that the calculations ob Bilby and Swinden, Tuba, and Rice and Rosengren are in accord with measured zone lengths, but none of the treatments examined provides a satisfactory description of the zone shape. The experiments also provide insights to the level of strain within the zone, and suggest that $\left|\frac{K}{Y}\right| \frac{1}{t} = 1$ or $\rho = \frac{t}{4}$ may be a useful upper bound for the plane strain regime.

DD FORM 1 JAN 64 1473

Security Classification

14. KEY WORDS	LINK A		LINK B		LINK C	
	ROLE	WT	ROLE	WT	ROLE	WT

INSTRUCTIONS

1. ORIGINATING ACTIVITY: Enter the name and address of the contractor, subcontractor, grantee, Department of Defense activity or other organization *(corporate author)* issuing the report.

2a. REPORT SECURITY CLASSIFICATION: Enter the overall security classification of the report. Indicate whether "Restricted Data" is included. Marking is to be in accordance with appropriate security regulations.

2b. GROUP: Automatic downgrading is specified in DoD Directive 5200.10 and Armed Forces Industrial Manual. Enter the group number. Also, when applicable, show that optional markings have been used for Group 3 and Group 4 as authorized.

3. REPORT TITLE: Enter the complete report title in all capital letters. Titles in all cases should be unclassified. If a meaningful title cannot be selected without classification, show title classification in all capitals in parenthesis immediately following the title.

4. DESCRIPTIVE NOTES: If appropriate, enter the type of report, e.g., interim, progress, summary, annual, or final. Give the inclusive dates when a specific reporting period is covered.

5. AUTHOR(S): Enter the name(s) of author(s) as shown on or in the report. Enter last name, first name, middle initial. If military, show rank and branch of service. The name of the principal author is an absolute minimum requirement.

6. REPORT DATE: Enter the date of the report as day, month, year; or month, year. If more than one date appears on the report, use date of publication.

7a. TOTAL NUMBER OF PAGES: The total page count should follow normal pagination procedures, i.e., enter the number of pages containing information.

7b. NUMBER OF REFERENCES: Enter the total number of references cited in the report.

8a. CONTRACT OR GRANT NUMBER: If appropriate, enter the applicable number of the contract or grant under which the report was written.

8b, 8c, & 8d. PROJECT NUMBER: Enter the appropriate military department identification, such as project number, subproject number, system numbers, task number, etc.

9a. ORIGINATOR'S REPORT NUMBER(S): Enter the official report number by which the document will be identified and controlled by the originating activity. This number must be unique to this report.

9b. OTHER REPORT NUMBER(S): If the report has been assigned any other report numbers *(either by the originator or by the sponsor)*, also enter this number(s).

10. AVAILABILITY/LIMITATION NOTICES: Enter any limitations on further dissemination of the report, other than those imposed by security classification, using standard statements such as:

(1) "Qualified requesters may obtain copies of this report from DDC."

(2) "Foreign announcement and dissemination of this report by DDC is not authorized."

(3) "U. S. Government agencies may obtain copies of this report directly from DDC. Other qualified DDC users shall request through
________________________________."

(4) "U. S. military agencies may obtain copies of this report directly from DDC. Other qualified users shall request through
________________________________."

(5) "All distribution of this report is controlled. Qualified DDC users shall request through
________________________________."

If the report has been furnished to the Office of Technical Services, Department of Commerce, for sale to the public, indicate this fact and enter the price, if known.

11. SUPPLEMENTARY NOTES: Use for additional explanatory notes.

12. SPONSORING MILITARY ACTIVITY: Enter the name of the departmental project office or laboratory sponsoring *(paying for)* the research and development. Include address.

13. ABSTRACT: Enter an abstract giving a brief and factual summary of the document indicative of the report, even though it may also appear elsewhere in the body of the technical report. If additional space is required, a continuation sheet shall be attached.

It is highly desirable that the abstract of classified reports be unclassified. Each paragraph of the abstract shall end with an indication of the military security classification of the information in the paragraph, represented as *(TS)*, *(S)*, *(C)*, or *(U)*.

There is no limitation on the length of the abstract. However, the suggested length is from 150 to 225 words.

14. KEY WORDS: Key words are technically meaningful terms or short phrases that characterize a report and may be used as index entries for cataloging the report. Key words must be selected so that no security classification is required. Identifiers, such as equipment model designation, trade name, military project code name, geographic location, may be used as key words but will be followed by an indication of technical context. The assignment of links, roles, and weights is optional.

NATIONAL ACADEMY OF SCIENCES - NATIONAL RESEARCH COUNCIL

DIVISION OF ENGINEERING

This project has been conducted under the advisory guidance of the Ship Research Committee of the National Academy of Sciences-National Research Council. The Committee assumes such cognizance of projects in materials, design and fabrication as relating to improved ship structures, when such activities are accepted by the Academy and assigned through its Maritime Transportation Research Board. In addition, this committee recommends research objectives and projects; provides liaison and technical guidance to such studies; reviews project reports; and stimulates productive avenues of research.

SHIP RESEARCH COMMITTEE

Chairman: M. L. Sellers, (I, II, III)
Naval Architect
Newport News Shipbuilding and Drydock Co.

Vice Chairman: J. M. Frankland (I, II, III)
(Retired) Mechanics Division
National Bureau of Standards

Members

W. H. Buckley (I, II)
Chief, Structural Criteria
Bell Aerosystems Co.

B. B. Burvank (III)
(Retired) Chief Metallurgist
and Chemist
Bath Iron Works Corp.

D. P. Clausing (III)
Senior Scientist
U. S. Steel Corporation

D. P. Courtsal (II, III)
Principal Hull Design Engineer
Dravo Corporation

A. E. Cox (I, II)
LHA Project Director
Newport News Shipbuilding
and Drydock Co.

F. V. Daly (III)
Manager of Welding
Newport News Shipbuilding
and Drydock Co.

J. F. Dalzell (I)
Senior Research Scientist
Hydronautics Incorporated

J. E. Goldberg (I) (II)
School of Civil Engineering
Purdue University

J. E. Herz (I, II)
Chief Structural Design Engineer
Sun Shipbuilding & Drydock Co.

G. E. Kampschaefer, Jr. (III)
Manager, Application Engineering
ARMCO Steel Corp.

B. R. Noton (II, III)
Visiting Professor
Dept. of Aeronautics and Astronautics
Stanford University

W. W. Offner (III)
Consulting Engineer

S. T. Rolfe (III)
Section Supervisor
U. S. Steel Corporation

M. Willis (I)
Assistant Naval Architect
Sun Shipbuilding and Drydock Co.

R. A. Yagle (II)
Marine Engineering
University of Michigan

(I) - Advisory Group I, Ship Strain Measurement & Analysis
(II) - Advisory Group II, Ship Structural Design
(III) - Advisory Group III, Metallurgical Studies

R. W. Rumke
Executive Secretary

SHIP STRUCTURE COMMITTEE PUBLICATIONS

These documents are distributed by the Clearinghouse, Springfield, Va. 22151. These documents have been announced in the Technical Abstract Bulletin (TAB) of the Defense Documentation Center (DDC), Cameron Station, Alexandria, Va. 22314, under the indicated AD numbers.

SSC-179, *Residual Strains and Displacements within the Plastic Zone Ahead of A Crack* by J. Cammett, A. R. Rosenfield, and G. T. Hahn. November 1966. AD 644815.

SSC-180, *Experimental Determination of Plastic Constraint Ahead of a Sharp Crack under Plane-Strain Conditions* by G. T. Hahn and A. R. Rosenfield. December 1966. AD 646034.

SSC-181, *Results from Full-Scale Measurements of Midship Bending Stresses on Two Dry-Cargo Ships- Report #2* D. J. Fritch, F. C. Bailey, J. W. Wheaton. March 1967. AD 650239.

SSC-182, *Twenty Years of Research under the Ship Structure Committee* by A. R. Lytle, S. R. Heller, R. Nielsen, Jr., and John Vasta. December 1967. AD 663677.

SSC-183, *Metallurgical Structure and the Brittle Behavior of Steel* by Morris Cohen. May 1968. AD 670574.

SSC-184, *Exhaustion of Ductility in Compressed Bars with Holes* by S. Kabayashi and C. Mylonas. June 1968. AD 670487

SSC-185, *Effect Of Surface Condition On The Exhaustion Of Ductility By Cold or Hot Straining* by J. Dvorak and C. Mylonas. July 1968. AD 672897.

SSC-186, *On The Effect Of Ship Stiffness Upon The Structural Response of A Cargo Ship To An Empulsive Load.* by Manley St. Denis and Samuel N. Fersht. September 1968. AD 675639.

SSC-187, *Biennial Report of Ship Structure committee.* September 1968. AD 675022.

SSC-188, *Effect of Repeated Loads on the Low Temperature Fracture Behavior of Notched and welded Plates* by W. H. Munse, J. P. Cannon and J. F. Kiefner. October 1968. AD 676722.

SSC-189, *The Video Tape Recording of Ultrasonic Test Information* by Robert A. Youshaw, Charles H. Dyer and Edward L. Criscuolo. October 1968.

SSC-190, *Bending Moment Distribution In AMariner Cargo Ship Model In Regular And Irregular Waves of Extreme Steepness* by Naresh M. Maniar and Edward Numata. November 1968.

SSC-191, *Plastic Flow In The Locale On Notches And Cracks In Fe-3Si Steel Under Conditions Approaching Plane Strain* by G. T. Hahn and A. R. Rosenfield. November 1968.